2009-07-09

Relaxation of Vibrationally Excited Trifluorobenzene and Tetrafluorobenzene by Collisions with Carbon Dioxide

Alan M. Johnson
Brigham Young University - Provo

Relaxation of Highly Vibrationally Excited Trifluorobenzene and Tetrafluorobenzene by Collisions with CO_2

By

Alan Marshall Johnson

A thesis submitted to the faculty of

Brigham Young University

In partial fulfillment of the requirements for the degree of

Masters of Science

Department of Chemistry and Biochemistry

Brigham Young University

August 2009

Brigham Young University

Graduate Committee Approval

of a thesis submitted by

Alan Marshall Johnson

This thesis has been read by each member of the following committee and by majority vote has been found satisfactory.

_____	_____
Date	Eric T. Sevy, Chair
_____	_____
Date	Matthew S. Asplund
_____	_____
Date	David V. Dearden
_____	_____
Date	Steven R. Goates
_____	_____
Date	Jaron C. Hansen

Brigham Young University

As chair of the candidate's graduate committee, I have read the thesis of Alan Marshall Johnson in its final form and have found that (1) its format, citations, and bibliographical style are consistent and acceptable and fulfill university and department style requirements; (2) its illustrative materials including figures, tables, and charts are in place; and (3) the final manuscript is satisfactory to the graduate committee and is ready for submission to the university library.

_____ _____

Date Eric T. Sevy,

Chair, Graduate Committee

Accepted for the Department

_____

David V. Dearden

Graduate Coordinator

Accepted for the College

_____

Thomas W. Sederberg

Associate Dean, College of Physical

and Mathematical Sciences

Abstract

Relaxation of highly vibrationally excited trifluorobenzene and tetrafluorobenzene by collisions with CO_2

Alan Marshall Johnson

Department of Chemistry and Biochemistry

Masters of Science

An investigation into the relaxation of highly vibrationally excited trifluorobenzene and tetrafluorobenzene following collisions with carbon dioxide was performed using diode laser transient absorption spectroscopy. A 248 nm excimer laser prepared the vibrationally hot (E'~41,000 cm^{-1}) fluorobenzene molecules. Large amounts of translational and rotational energy are transferred through collisions between the hot donor molecule and CO_2. Rate constants and collisional probabilities were calculated by probing the high J states (J=58~80) of CO_2 in the vibrational ground state, 00^00, with measurements taken 1 μsec, ¼ the mean gas collision time, following each excimer laser pulse. The energy transfer probability distribution function, *P(E,E')*, was calculated for each molecule using the state-resolved probabilities and the energy gain of the bath. The study found a relationship between the fraction of strong collisions and the donor's dipole moment. Additionally, these findings support an application of Fermi's Golden rule to collisional energy transfer by linking the shape of *P(E,E')* to the shape of the donor's density of states as a function of ΔE.

Acknowledgements

I would like to begin by thanking my wife Shelley for her constant support and her loving patience while I attended graduate school; I could not have asked for a better companion. I also thank my parents for offering support in so many ways and for emphasizing education while I was young. I sincerely thank Dr. Sevy for his patience in teaching and willingness to be a mentor to me in the laboratory. I cannot express enough gratitude for the opportunity to work with him. I offer my appreciation for his unique teaching style that was key to my growth as a student. I also wish to thank him for the many hours spent reviewing this thesis and making corrections. I felt it a privilege to work with him and be a student of him. I am grateful to Kilyoung Kim, my fellow graduate student, whom I spent a great deal of time with in the lab performing experiments, as well as, the many classes and assignments that we faced together. I often joked that I spent more time with Kim than my own wife, and I know several weeks where that was certainly the case. I give thanks to all those who worked with me in the lab: Leah Hall, Kortney Judd, Debbie Mitchell, Maurine Mayhew, Amber Powell, and Karen Richards. Thank you for the many hours spent doing and often redoing experiments and computations. Thank you to the department of Chemistry and Biochemistry and for the many members of faculty that I worked with and who were so willing to offer help to me. I would specifically like to thank Dr. Philip Brown for giving me the opportunity to teach the Chem 107 lab course for so many semesters. This was a tremendous growing experience for me and one that I will cherish, surprisingly, for the rest of my life. Finally, I am grateful to the Church and to Brigham Young University for a place where learning, both secular and spiritual, can take place.

Table of Contents

Table of Figures

List of Tables

Chapter 1

Introduction

1.1 Background

Thermal unimolecular reactions find application in many fields, for example atmospheric and combustion chemistry.[1] Studies to understand these types of reactions date back to the early part of the 20th century beginning with Perrin[2] who proposed thermal unimolecular reactions were fueled by radiation absorption through the walls of the reaction vessel. Two observations[3] are not accounted for through the radiation absorption hypothesis. First, the rate should be dependent on the surface area of the reaction vessel, and second, at low pressures the same reaction rate should be sustained because the amount of radiation remains constant. Langmuir[4] tested Perrin's hypotheses by calculating the radiation flux the molecules would be exposed to and found radiation to not be a sufficient source of energy to drive the observed kinetics. The finding occurred due to limitations in the understanding of black-body radiation; if the same calculations were performed now, they would support the radiation absorption theory. Fortunately, the finding was used to refute the radiation theory and led scientists to continue searching for a better mechanism to explain thermal unimolecular reactions.

Lindemann,[5] three years after Perrin, proposed a new theory that could account for the limitations listed earlier for the radiation absorption model. Lindemann suggested that a molecule undergoes a bimolecular collision in which the reactant becomes activated with sufficient energy to proceed toward products. As part of the mechanism, an energized molecule could collide with another molecule before forming products. This collision would result in deactivating the molecule such that it no longer had sufficient energy to react. The proposed mechanism explained why unimolecular rates quickly dropped off at lower

pressures. The mechanism, introduced by Lindemann, is generally stated by the following reactions

$$\begin{aligned} A + Bath &\xrightarrow{k_1} A^* + Bath \\ A^* + Bath &\xrightarrow{k_{-1}} A + Bath \\ A^* &\xrightarrow{k_2} \text{Products} \end{aligned} \tag{1.1}$$

where A^* represents a molecule with sufficient energy to form into products and *Bath* is any molecule that collides with *A*.

The Lindemann model, though simple, helped scientists begin to understand how unimolecular reactions occurred. The model uses a few assumptions resulting in the shortcomings found in this mechanism. First of all, it is assumes that all collisions between *A* and *Bath* where *A* gains energy, will result in *A* being activated with enough energy to form products. This is not always true; each molecule has a differing amount of energy within a large distribution of energies. Frequently, a collision with *Bath* results in energy being transferred to *A* but not with the energy required for *A* to become activated such that it will form products. This "up" collision is therefore not an activating collision and is not accounted for in the model. Likewise, a "down" collision is not truly deactivating when energy is removed from A^* and retains sufficient energy to form products. Therefore, the rate constants for activating and deactivating collisions, as shown in eq 1.1, over estimate the rate of reaction.[3] Four years after Lindemann made this proposal, Hinshelwood[6] accounted for this simplification by adjusting the rate constant of product formation to be based on internal energy of *A* following a collision. This modification adjusted the final reaction step in eq 1.1 in the following way

$$A^*(E) \xrightarrow{k(E)} \text{Products}. \tag{1.3}$$

These two ideas combined are referred to as the Lindemann-Hinshelwood theory of thermal unimolecular reactions.

The low-pressure condition causes the energy transfer step in the Lindemann-Hinshelwood mechanism to become increasingly more involved in the rate of product reaction. An accurate description[7] of the energy of *A* over time is given by the master equation. This equation takes the following form:

$$\frac{d[A(E,t)]}{dt} = k_{coll}[Bath]\int_0^\infty \{P(E,E')[A(E',t)] - P(E',E)[A(E,t)]\}dE' - k_E[A(E,t)] \quad (1.4)$$

where *P(E,E′)* is the probability that a molecule with internal energy, *E′*, will be left with energy, E, after a collision. Breaking up the equation into three parts yields the three different reactions that take place: energized molecules produced through a collision; energized molecules that are lost as a result of collision, and energized molecules that are lost due to product formation. The research presented in this thesis is focused towards the initial gain of energy by molecule *A* constituting *P(E,E′)* with a change of energy greater than 2000 cm^{-1}.

Collisions that transfer large amounts of energy (>2000 cm^{-1}) are significant when considering the overall energy transfer picture.[8] These large collisional events were first observed through work by Steel[9] in the late '80's using perfluorobenzene. Interest in these collisions has lead to several computational[10,11] and experimental[9,12] studies designed to better understand how and why these collisions occur. Luther[13] used kinetically controlled selective ionization with toluene to find the existence of a large distribution of internal energies in the energized donor molecule which would result in a large distribution of collisional energy transfer. In light of these results, theorists performed classical trajectory

calculations to determine the distribution of probabilities for energy transfer, essentially *P(E,E')*. The resulting distribution function that resulted from these calculations represents the high ΔE tail of energy transfer; a single exponential function failed to accurately fit the data. Scientist found a double exponential function[14] to most accurately fit the data with one exponential representing strong collisions and the other depicting weak collisions.

1.2 Experimental Approach

Flynn[15] et al. were the first to experimentally measure *P(E,E')*; they developed a technique using transient IR probe spectroscopy.[16] The process uses an IR diode laser to measure energy transferred into a tractable bath molecule; the technique could be used for rotational, vibrational, and translational energy measurements by measuring the appropriate absorption transition. In the case of translational energy as found through probing the Doppler broadened lineshape, the method takes advantage of the resolution of the diode laser having a frequency with an order of magnitude smaller than the room temperature lineshape of the probe molecule transition.

Our lab uses a variation on this technique to measure rotational and translational energy gains in the bath;[17,18] a diagram of the experimental setup is given in Figure 1.1. A KrF excimer laser produces a 248nm pulse to electronically excite a donor molecule. Following rapid radiationless relaxation on a time scale several orders of magnitude faster than the collision time scale based on our experimental setup, the donor molecule collides with the bath resulting in a large transfer of energy. CO_2 is used in this experiment as the bath molecule fulfilling the requirement of being spectroscopically tractable. The experimental mechanism[15] as it occurs in our studies is detailed in the following reactions

$$\begin{aligned} Donor + h\nu(248nm) &\longrightarrow Donor^{E'} \\ Donor^{E'} + CO_2 &\longrightarrow Donor^{E'-\Delta E} + CO_2(00^00;J,V) \\ CO_2 + h\nu(4.3\mu m) &\longrightarrow CO_2(00^01;J\pm 1,V) \end{aligned} \tag{1.5}$$

where ΔE is the energy transferred from Donor to CO_2, J is the rotational quantum number, and V is the recoil velocity of scattered CO_2. The antisymmetric stretch of CO_2 for J= 58, 62, 70, 76, and 80 is probed in our experiments. In addition to the amount of energy transferred, the rate of scattering into these excited states is also required to calculate *P(E,E')*.

Experimentally obtained *P(E,E')* becomes more meaningful as it is fit to a double exponential allowing for a more specific comparison to be made. The double exponential function[8,19,20] used for fitting the experimental *P(E,E')* is

$$\begin{aligned} P(E,E') &= \frac{(1-f)\exp\{-(E'-E)/\alpha\} + f\exp\{-E'-E)/\gamma\}}{(1-f)(\alpha+\beta)+f(\gamma+\delta)}, \quad E \le E' \\ P(E,E') &= \frac{(1-f)\exp\{-(E-E')/\beta\} + f\exp\{-E-E')/\delta\}}{(1-f)(\alpha+\beta)+f(\gamma+\delta)}, \quad E > E' \end{aligned} \tag{1.6}$$

where α and γ are the average energy of weak and strong “down” collisions relative to the donor, respectively, β and δ are the average energy of weak and strong “up” collisions relative to the donor, respectively, and f is related to the fraction of strong collisions and will loosely be referred to as a ”fraction” . The “up” collision parameters are not necessary to directly measure as they are related to the “down” collision parameters through detailed balance.[19]

The thesis presented here is a compilation of two studies that are part of a comprehensive look at all the fluorobenzene derivatives. By looking at all the different fluorobenzenes, trends relating to density of states and low frequency modes can more easily be

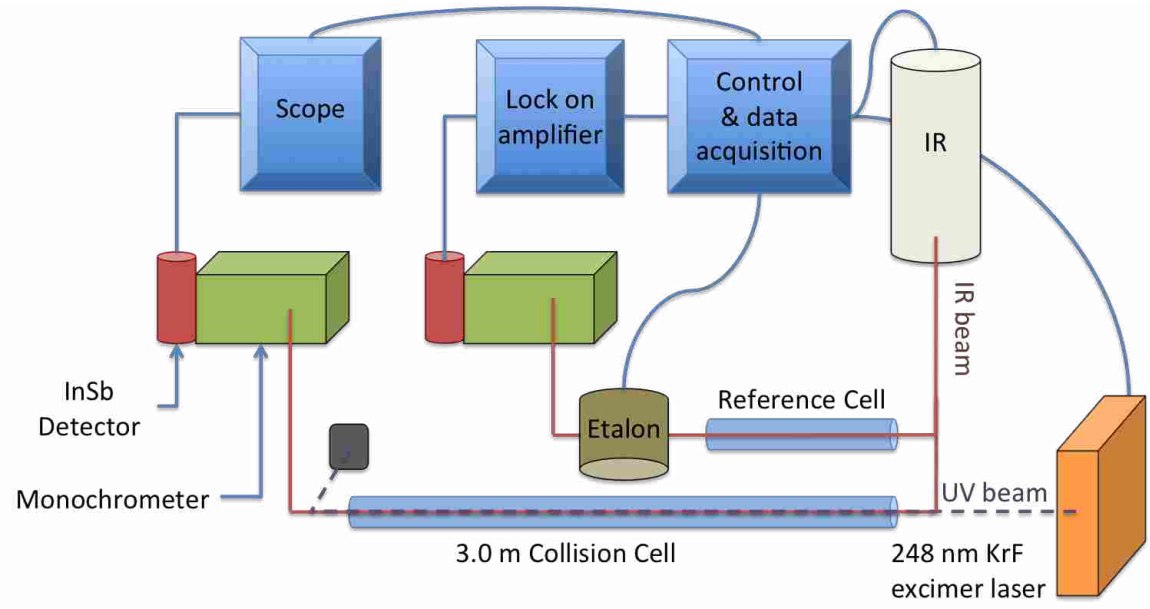

Figure 1.1: Experimental setup using 3.0 m collision cell with collinear high resolution IR beam and 248 nm excimer laser passing through a flowing 20.0 mtorr 1:1 donor to bath gas sample. An InSb detector is used for both the measurement path and reference path. The lock-on amplifier locks onto either the peak of interest for linestrength measurements or onto the fringe produced by the etalon when measuring lineshapes.

established. Comparing only a group of isomers identifies relationships dealing with frequency of individual modes or the effect of dipole moment on the shape of *P(E,E')*. The first study presents collisions between excited tetrafluorobenzene isomers with CO_2; the second study uses excited trifluorobenzene and its collisions with CO_2. Previous studies using the difluorobenzene isomers[17] and perfluorobenzene[21] as the energy transfer donor molecule are used for comparison. Our lab has completed studies of monofluorobenzene[22] and pentafluorobenzene[23] with the results awaiting publication.

1.3 References

1. Levine, R. D., *Molecular Reaction Dynamics*. Cambridge University Press: Cambridge, UK, 2005.
2. Perrin, J., *Annals of Physics* **1919,** *11*.
3. Steinfeld, J. I.; Francisco, J. S.; Hase, W. L., *Chemical kinetics and dynamics*. 2nd ed.; Prentice Hall: Englewood Cliffs, NJ, 1999; p 548.
4. Langmuir, I., *Journal of Chemical American Society* **1920,** *42*.
5. Lindemann, F. A., *Transactions of the Faraday Society* **1922,** *17*, 598-606.
6. Hinshelwood, C. N., *Proc. R. Soc. A* **1927,** *113*.
7. Troe, J., *J. Chem. Phys.* **1977,** *66*, 4745-4757.
8. Bernshtein, V.; Oref, I., *J. Phys. Chem.* **1993,** *97*, 12811-12818.
9. Hassoon, S.; Oref, I.; Steel, C., *J. Chem. Phys.* **1988,** *89*, 1743-1744.
10. Lendvay, G.; Schatz, G. C., *J. Phys. Chem.* **1990,** *94*, 8864-8866.
11. Brown, N. J.; Miller, J. A., *J. Chem. Phys.* **1984,** *80*, 5568-5580.

12. Morgulis, J. M.; Sapers, S. S.; Steel, C.; Oref, I., *J. Chem. Phys.* **1989,** *90*, 923-929.

13. Luther, K.; Reihs, K., *Ber. Bunsenges. Phys. Chem.* **1988,** *92*, 442-445.

14. Bollati, R. A.; Ferrero, J. C., *J. Phys. Chem.* **1994,** *98*, 3933-3936.

15. Mullin, A. S.; Michaels, C. A.; Flynn, G. W., *Journal of Chemical Physics* **1995,** *102* (15), 6032-6045.

16. Flynn, G. W.; Weston, R. E., Jr., *Journal of Physical Chemistry* **1993,** *97* (31), 8116-8127.

17. Mitchell, D. G.; Johnson, A. M.; Johnson, J. A.; Judd, K. A.; Kim, K.; Mayhew, M.; Powell, A. J.; Sevy, E. T., *Journal of Physical Chemistry A* **2008,** *112* (6), 1157-1167.

18. Johnson, J. A.; Kim, K.; Mayhew, M.; Mitchell, D. G.; Sevy, E. T., *Journal of Physical Chemistry A* **2008,** *112* (12), 2543-2552.

19. Troe, J., *J. Chem. Phys.* **1992,** *97*, 288-292.

20. Lenzer, T.; Luther, K.; Troe, J.; Gilbert, R. G.; Lim, K. F., *J. Chem. Phys.* **1995,** *103*, 626-641.

21. Michaels, C. A.; Lin, Z.; Mullin, A. S.; Tapalian, H. C.; Flynn, G. W., *Journal of Chemical Physics* **1996,** *106* (17), 7055-7071.

22. Kim, K.; Johnson, A. M.; Powell, A. L.; Mitchell, D. G.; Sevy, E. T., *Journal of Physical Chemistry A* **In Preparation**.

23. Kim, K.; Johnson, A. M.; Powell, A. L.; Mitchell, D. G.; Mayhew, M.; Judd, K. A.; Hall, L.; Richards, K.; Sevy, E. T., *Journal of Chemical Physics* **In Preparation**.

Chapter 2

Collisional Relaxation of the Three Vibrationally Excited Tetrafluorobenzene Isomers by Collisions with CO_2

2.1 Introduction

Scientists have shown interest for over 90 years in mechanisms for energy transfer processes in part due to their relationship to thermal unimolecular reactions.[1] In unimolecular reactions, collisional energy transfer[2] plays a critical role in the initial step of activating a molecule before it can form product. Energy transfer that occurs with a molecule containing chemically significant amounts of energy, with a high density of states has been of particular importance.[3] Understanding how energy is transferred over time has led to the development[4] of an energy transfer probability distribution function or *P(E,E′)*. This function, which gives the probability that a molecule with energy E′ will have energy E following a single collision, has been shown to influence the rate of unimolecular reactions in the fall off regime. The importance of *P(E,E′)* has been known for several decades, but only in the last 15 years[5,6] have studies been done that experimentally measured this function. Other techniques[7-10] followed this initial discovery and have led to greater insights concerning the relationship between molecular parameters and *P(E,E′)*.

Early studies of energy transfer monitored energy loss from the donor molecule; their technique could not be used to measure *P(E,E′)* for complex molecules with chemically significant amounts of energy. Our lab uses an alternative approach by following the transient IR probe technique that was first developed by Flynn[11,12] and is now in use by our lab[13,14] and by the Mullin group[15,16]. The technique excites a donor molecule that then undergoes a single collision with a bath molecule whose distribution of translational and rotational energies can be tracked. One could attempt to track the energy change of the donor, but due to the large density of states, using a simple bath molecule is more practical

as the final energy states following a single collision can be spectroscopically resolved. Our studies use CO_2 as the bath molecule because its rovibrational spectrum is well known; other studies[17] have also used H_2O, HOD, and HCl. Mullin[18] has used a variation of the technique to specifically measure V→V and V→RT energy transfer pathways. Tracking velocity distributions is made possible through the use of a high resolution IR diode laser. CO_2 has a room temperature linewidth of $\Delta\nu$=0.0042 cm^{-1} and the laser has a frequency resolution of $\Delta\nu$=0.0003 cm^{-1}; because the linewidth is considerably larger than the frequency width of the IR diode laser, one can measure the number of molecules scattered into a rovibrational state, their recoil velocity, and the rate constant for this process. These state resolved measurements[11] allow for the calculation of *P(E,E')*.

The purpose of many of these studies was to compare the shape of *P(E,E')* to molecular parameters. Comparisons are made by using a model function with parameters that relate information about the shape. The model that best fits the shape of *P(E,E')* is a double exponential function[19] with parameters representing the average energy of weak and strong collisions. Several studies[12,20] have shown that these parameters, and thus the shape of *P(E,E')*, to largely be governed by the donor molecule's density of states. One other parameter of importance loosely relates the fraction of large ΔE collisions.[12] Previous studies have shown that this "fraction" is related to the number of low frequency modes (ν<500 cm^{-1}) in the donor[21].

In addition to *P(E,E')*, Sevy and coworkers[12,14,21] have developed a function that relates the number of molecules that can transfer a set amount of energy out of a particular vibrational mode, based on the fraction of molecules in that mode with the determined amount of energy, along with the efficiency of that mode which is related to its frequency,

The function is referred to as the "fractional energy transfer distribution," *f(E,E')*, model. The model follows a similar shape as *P(E,E')* when choosing a dominant energy transfer mode is chosen and has therefore proven useful in determining which modes are most responsible for the shape of *P(E,E')*. Quantum scattering calculations[22] between benzene and helium showed that most of the energy transferred in a collision is "leaked out" of only certain modes. These modes were found to have low frequency and out-of-plane motion giving them large energy transfer cross sections. Lendvay[23] furthered this work through classical trajectory studies on CS_2 and found similar results. The study confirmed Clary's observations of only certain modes being responsible for a majority of energy transfer. Lendvay referred to these as gateway modes or conduits where a majority of the energy is leaked to the bath. A study[13] of the difluorobenzene isomers performed by our lab found these gateway modes for energy transfer to be consistent with C_6F_6.

This study joins with others as part of a larger more comprehensive work to analyze the collisional energy transfer between all the fluorobenzene derivatives with CO_2. C_6F_6 and the difluorobenzene (DFB) isomers have been reported previously.[6,13] Here we present collisional studies between the three isomers of tetraflurobenzene (TetraFB), 1234-Tetrafluorobenzene, 1235-tetrafluorobenzene, and 1245-tertrafluorobenzene with CO_2. These studies will help to better understand what molecular parameters have the greatest influence on the shape and magnitude of *P(E,E')*. The molecules in question all have the same number of vibrational modes with similar motion and also have strong similarities in their initial energy and chemical make-up. As the number of differences between molecules is minimized, changes in *P(E,E')* can be more accurately linked to molecular properties.

2.2 Experiment

The UV pump, IR probe technique used to study the collisional relaxation of the three isomers of tetrafluorobenzene has been described in detail elsewhere;[11,24,25] therefore, only a brief outline of the method is presented here. A 1:1 mixture of gas phase tetrafluorobenzene and CO_2 flows through a 3.0 m collision cell at a total pressure of ~20 mTorr. A 248 nm KrF excimer laser (Lamda Physik CompEx 201) generates excited TetraFB through the $S_1 \leftarrow S_0$ transition. Electronically excited tetrafluorobenzene then undergoes a rapid radiationless internal conversion into vibrationally excited states in the ground electronic state, $S_1 \rightarrow S_0^*$. Energy gain into individual rotational states of CO_2 (00^00, J=58, 62, 70, 76, and 80) resulting from collisions with hot tetrafluorobenzene in S_0^* is monitored by probing the transient absorption of IR light (λ= 4.3 μm) that is collinearly propagated with the UV beam through the collision cell. The highly resolved (0.0003 cm^{-1}) IR laser (Laser Components) is used to probe the scattered CO_2 molecules via the antisymmetric stretch transition. To insure that only a single diode laser mode is detected, the infrared light passes through a single grating monochromator (Acton Spectra pro 500i) before being focused onto a liquid nitrogen cooled InSb detector. Two types of measurement are collected: the transient fractional absorption $\Delta I/I_0$ at 1 μs (mean collision time is 4 μs) and the full width at half max (FWHM) of each of the rotational states. From these two measurements, we determine the amount of energy gained by CO_2. The increase in CO_2 translational energy is determined through the Doppler broadened linewidths of each rotational peak.

For linecenter measurements, a reference CO_2 signal is created by removing 4% of IR light that passes through a CO_2 reference cell into a second monochromator and detector

in order to keep the laser frequency constant. For FWHM measurements, the laser is locked onto a scanning Fabry-Perot Etalon fringe. The fringe is moved using a DAC that is calibrated between two peaks of known frequency in the reference cell. The etalon is then used to scan 40 evenly distributed frequencies across the entire rovibrational lineshape that are averaged over 100 laser shots. Linestrengths at the center of the ro-vibrational line are measured by locking the frequency of the diode to a CO_2 reference peak. Rate constant data is obtained from the linecenter and linewidth measurements. However, due to the divergence of the excimer beam, the rate constants are only relatively accurate. A calibration experiment[21] is also performed which scales experimentally obtained rate constants for pyrazine with literature values.[26] The same scaling factor is then applied to rate constants measured for each tetrafluorobenzene isomer under the same conditions. This scaling allows for consistent comparisons across all isomers and with other molecules.

The 1,2,3,4-tetraflurobenzene (Aldrich, 99% purity), 1,2,3,5-tetrafluorobenzene (Aldrich 95% purity) and 1,2,4,5-tetrafluorobenzene (99% purity) were purified prior to our experiments using the freeze-pump-thaw method.

2.3 Results

2.3.1 Rotational and Translational Excitation of Carbon Dioxide Bath.

Transient CO_2 populations of various rotational states between J=58 and 80 in the ground vibrational level(00^00) were measured using infrared absorption following 248 nm UV excitation of 1234-tetraFB, 1235-tetraFB, and 1245-tetraFB. Because the CO_2 rotational and translational energies change with each collision, the distributions probed at short times after the excimer laser pulse represent the nascent single collision dynamics without

significant relaxation. Transient signals for the p70 {(00^01, J=69) ← (00^00, J=70)} CO_2 transition at 2279.8391 cm^{-1}, as a result of collisions with each of the fluorinated benzenes investigated in this study, are shown plotted as a function of time relative to the excimer laser pulse in Figure 2.1. The signals represent the average of 100 laser shots fired into a 1:1 flowing 20.0 mTorr gas mixture of CO_2 and tetrafluorobenzene. Following a laser pulse, CO_2 molecules are scattered into rotationally excited states by collisions with the excited donor molecules. By taking a measurement at 1 μsec, which represents one fourth of the mean gas collision time, only single collisions between donor and bath are significant. The data at times greater than 4 μsec are much more complicated because the state continues to fill due to additional collisions with slightly thermalized TetraFB molecules as well as CO_2 molecules in higher rotational states relaxing into the state being probed. The population at later times decreases through CO_2 molecules undergoing relaxation out of the high angular momentum states. The similarity between transients indicates that similar numbers of CO_2 molecules are scattered into this state by each donor. Measured absorptions are converted[27] to CO_2 number density using absorption line strengths found in the HITRAN spectroscopic database.[28]

Figure 2.2 shows a Boltzmann plot of the rotational state distribution of CO_2 following a collision with TetraFB. A linear relationship observed over this set of J states allows us to use a single temperature to describe each distribution. The temperatures obtained for CO_2 following collisions with 1234-, 1235- and 1245-TetraFB are 940 ± 120K, and 920±70K, 870 ± 110K, respectively. These values are consistent with rotational temperatures of high-J tails found in previous studies of other fluorinated benzene molecules (C_6H_6: 795 K[6]; $C_6H_4F_2$: isomers 930, 970, and 1020 K[13]). It is important to note

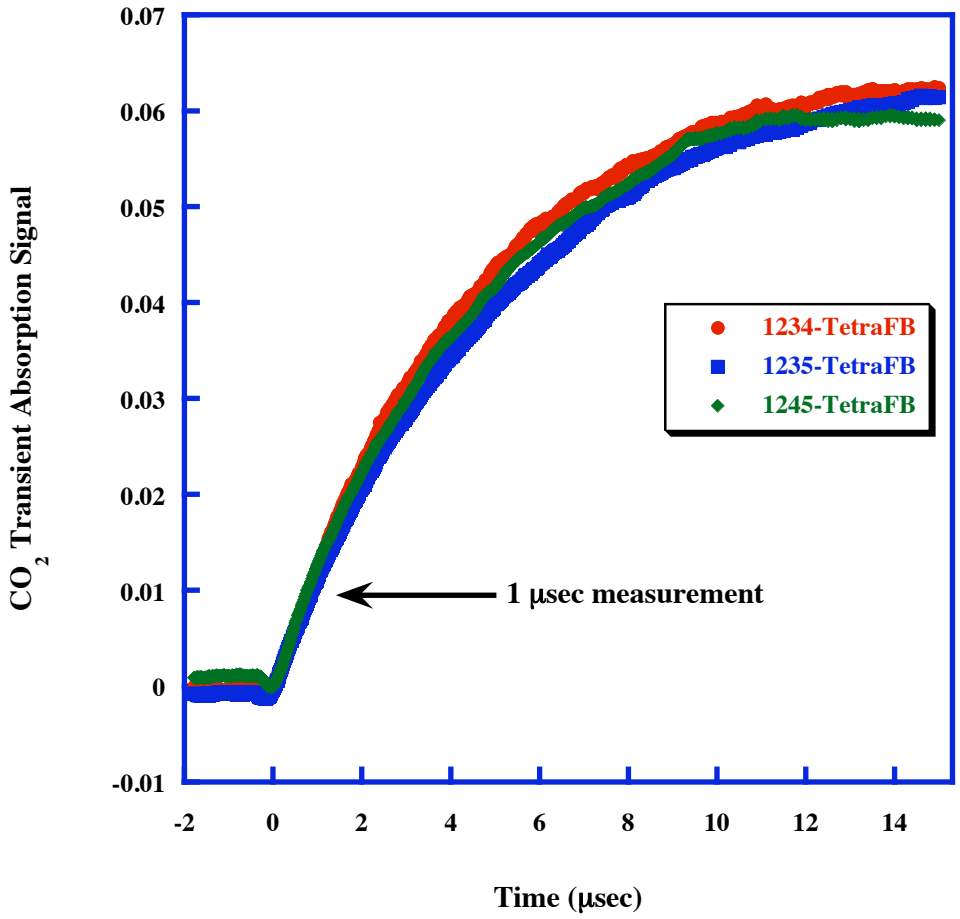

Figure 2.1: The fractional IR absorption of CO_2 collisionally scattered into the 00^00, J=70 state as a function of time following UV excitation of the three isomers of tetrafluorobenzene (TetraFB). To ensure that the measured energy transfer parameters represent single collision events, transient signals are measured at 1 μsec (1/4 the mean collision time) following a laser pulse of a flowing gas mixture of 10 mtorr CO_2 and 10 mtorr of 1,2,3,5- TetraFB (blue), 1,2,4,5-TetraFB (green) or 1,2,3,4-TetraFB (red).

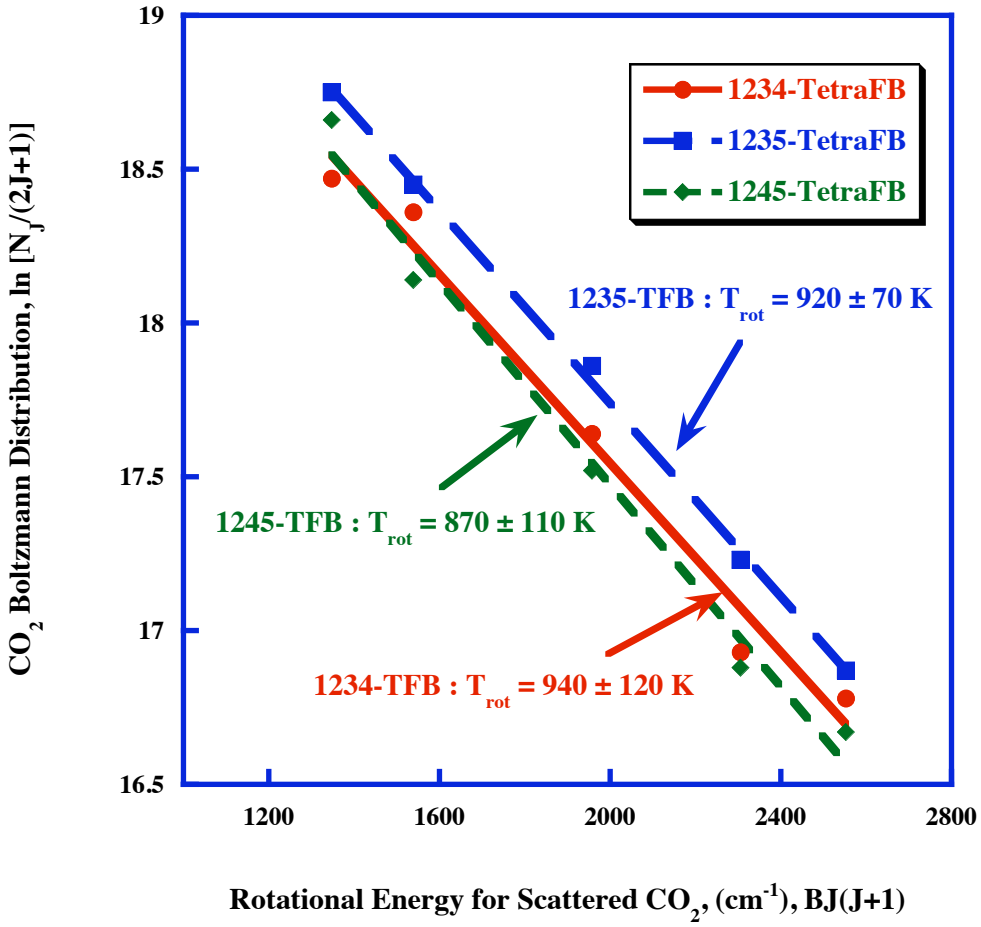

Figure 2.2: Boltzmann plot of the nascent rotational distributions in the ground vibrational level of CO_2 following excitation by single collisions with vibrationally hot 1,2,3,5- TetraFB (blue), 1,2,4,5-TetraFB (green) or 1,2,3,4-TetraFB (red). Points are calculated from the factional absorption of CO_2 at 1 μsec after UV excitation of donor. The solid lines are the best linear least squares fit to the experimental points measured over the range J = 58 to 80. The slope of the best fit line is equal to $-1/k_B T_{rot}$ and the number densities, N_J, are in units of molecules/cm^3. The rotational temperature for CO_2 molecules scattered into the high J states following collisions with 1,2,3,4-, 1,2,3,5-, and 1,2,4,5-TetraFB is 940 ± 120 K, 920 ± 70 K and 870 ± 110 K, respectively. Error represents 95% confidence limits.

that this distribution is not representative of all states; rather it describes the distribution over the states of the high-J tail and not necessarily of those in the low-J tail.

Doppler Broadened line shapes are measured to determine the velocity distribution of CO_2 molecules in the excited J state following collisions with TetraFB. In Figure 2.3a, a Doppler broadened line shape for CO_2 following a single collision with 1234-TetraFB is measured by averaging the transient signal at 1 μsec after the laser pulse at 40 equally spaced frequencies across the p70 transition for CO_2. The distribution of recoil velocities is most accurately fit to a Gaussian distribution; therefore, a single translational temperature, which is related to the full width at half maximum (FWHM), accurately describes this distribution. A FWHM of 0.0081 ± 0.0003 cm^{-1} is calculated from the Gaussian fitting parameters for this transition giving a T_{trans} of 1090K. Figures 2.3b and 2.3c represent lineshapes of the p70 transition for the reaction mixtures of 1235-TetraFB and 1245-TetraFB with CO_2 respective and give T_{trans} values of 1160 K and 810 K respectively. These linewidths are about two times the value of 0.0042 cm^{-1} obtained for a room temperature distribution of CO_2, signifying that a large amount of vibrational energy is transferred from the donor and converted to translational energy in CO_2.

Linewidths for CO_2 J=58 to J=80 were measured and are tabulated in Table 2.1, along with translational temperatures corresponding to each linewidth. Translational temperatures are given in both lab frame and center of mass frame. Center of mass frame, however, more accurately describes the amount of energy transferred in each collision. Figure 2.4 graphically represents the translational temperatures plotted vs. J state; the right axis gives the center of mass temperatures and the left axis correlates FWHM in

Figure 2.3: Nascent Doppler broadened lineshapes for the absorption transition CO_2 (00^00; J=70) → CO_2 (00^01; J=69) obtained by probing CO_2 molecules excited by collisions with vibrationally excited (a) 1,2,3,4-, (b) 1,2,3,5- and (c) 1,2,4,5-TetraFB. The lineshapes were obtained using a flowing mixture of 10 mTorr CO_2 and 10 mTorr TetraFB. The points represent the fractional IR absorption of CO_2 collisionally scattered into the 00^00, J=70 state measured 1 μsec following 248 nm excimer laser pumping of TetraFB. Absorption measurements are averaged over approximately 40 transient signals at each diode laser frequency across the line. The solid lines are the best non-linear least squares fit to a Gaussian function. The full width at half maximum (FWHM) obtained from the measured lineshapes is 0.0081 ± 0.0003, 0.0084 ± 0.0005, and 0.0070 ± 0.0019 cm^{-1} for 1,2,3,4-, 1,2,3,5-, and 1,2,4,5- TetraFB, respectively. For comparison, the FWHM of a CO_2 lineshape with T_{trans} = 300 K is approximately 0.0042 cm^{-1}. The final translational temperature, T_{trans}, is related to the linewidth, $\Delta\nu_0$ (full width at half maximum) through the expression $T_{trans}(K)=[mc^2(\Delta\nu_{obs})^2]/[8Rln2(\nu_0)^2]$, where m is the mass of CO_2, c is the speed of light, R is the gas constant, and ν_0 is the wavenumber at the center of the absorption line.

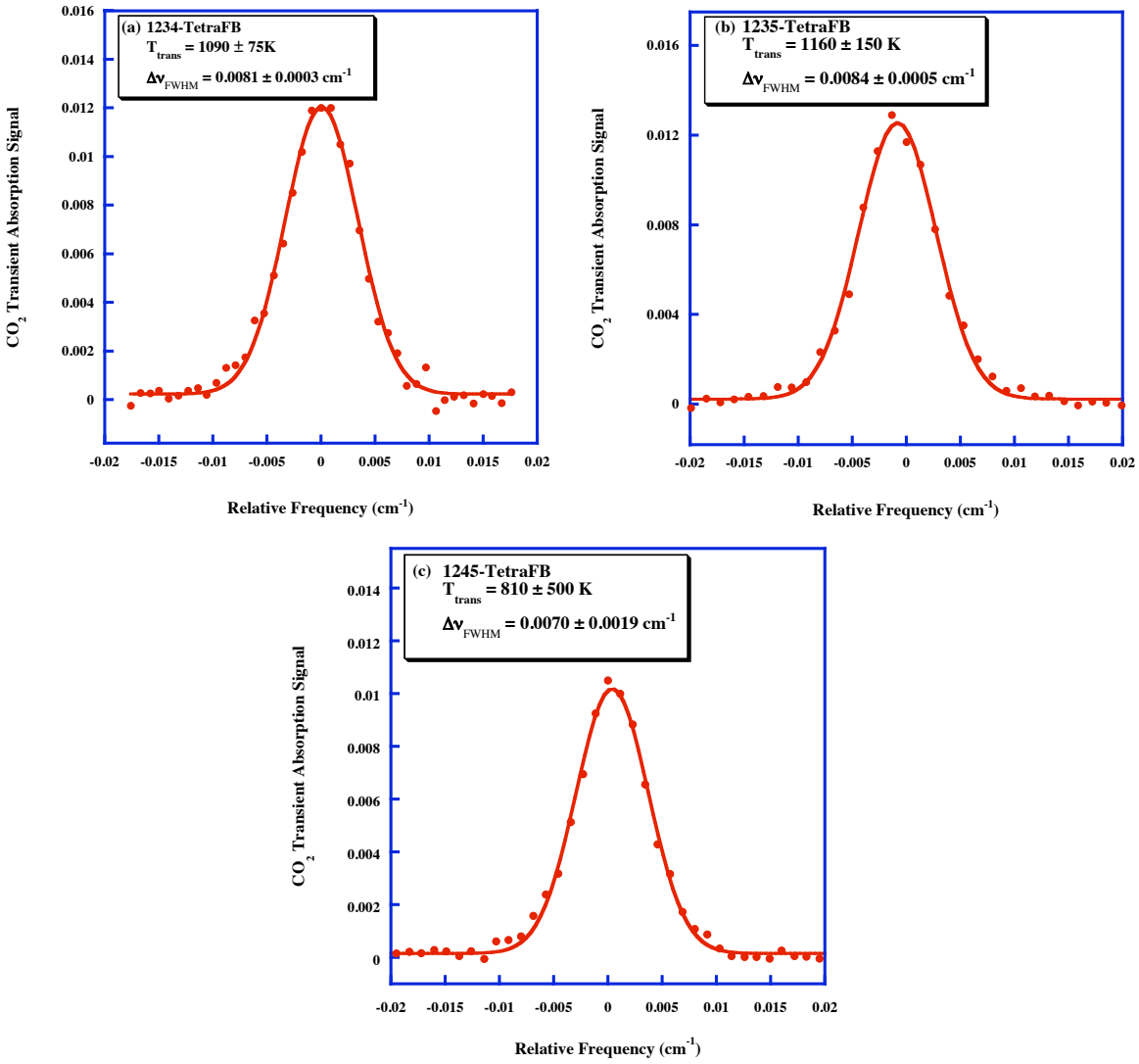
(a) 1234-TetraFB
T trans = 1090 ± 75K
Δν FWHM = 0.0081 ± 0.0003 cm-1
(b) 1235-TetraFB
T trans = 1160 ± 150 K
Δν FWHM = 0.0084 ± 0.0005 cm-1
(c) 1245-TetraFB
T trans = 810 ± 500 K
Δν FWHM = 0.0070 ± 0.0019 cm-1
CO2 Transient Absorption Signal
Relative Frequency (cm-1)

Table 2.1: Full width at half Maximum Doppler linewidths,[a] translational temperatures,[b] and center of mass translational temperatures[c] with uncertainty[d] for $CO_2(00^00, J)$ following collisions with highly vibrationally excited 1,2,3,4-tetrafluorobenzene[E'], 1,2,3,4-tetrafluorobenzene[E'], and 1,2,3,4-tetrafluorobenzene[E'].[e]

CO_2	1,2,3,4-tetrafluorobenzene			1,2,3,5-tetrafluorobenzene			1,2,4,5 tetrafluorobenzene		
$(00^00,J)$[f]	$\Delta\nu_{obs}$, (cm^{-1})[a]	T_{trans}, K[b]	T_{trans}^{COM}, K[c]	$\Delta\nu_{obs}$, (cm^{-1})[a]	T_{trans}, K[b]	T_{trans}^{COM}, K[c]	$\Delta\nu_{obs}$, (cm^{-1})[a]	T_{trans}, K[b]	T_{trans}^{COM}, K[c]
58	0.0053±0.0006	460±50	510±60	0.0057±0.0010	540±190	610±250	0.0059±0.0004	570±70	650±90
62	0.0071±0.0009	820±230	970±300	0.0060±0.0007	590±150	670±190	0.0051±0.0008	430±140	470±180
70	0.0081±0.0003	1090±75	1320±100	0.0084±0.0005	1160±150	1410±190	0.0070±0.0019	810±500	970±650
76	0.0085±0.0006	1190±190	1450±240	0.0096±0.0004	1500±160	1870±190	0.0082±0.0013	1130±400	1370±490
80	0.0112±0.0019	2080±790	2610±1010	0. 0109±0.0009	2000±320	2500±420	0.0094±0.0016	1630±390	2020±500

Table 2.1 continued

[a] The measured full width at half maximum (FWHM) of the transient Doppler linewidths for the $CO_2(00^00,J) \rightarrow CO_2(00^01,J-1)$ transition, determined at 1 μs after tetrafluorobenzene excitation in a 1:1 sample of tetrafluorobenzene:CO_2 at a total pressure of 20 mTorr. FWHM is obtained from fitting the experimentally determined Doppler lineshapes with a Gaussian function. The thermal Doppler linewidth for CO_2 at T=298 K is $\Delta\nu_0$ =0.0042 cm^{-1}. [b] The final translational temperature, T_{trans}, is calculated from the linewidth, $\Delta\nu_0$ (FWHM), using the expression $T_{trans}(K)=[mc^2(\Delta\nu_{obs})^2]/[8R\ln 2(\nu_0)^2]$, where m is the mass of CO_2, c is the speed of light, R is the gas constant, and ν_0 is the wavenumber at the center of the absorption line. [c] The final center of mass temperature, T_{trans}^{COM}, is obtained from the expression $T_{trans}^{COM}(K) = T_{trans}^{CO_2} + (T_{trans}^{CO_2} - T)(m_{CO_2}/m_{tetrafluorobenzene})$, where $T_f^{CO_2}$ is the temperature describing the CO_2 lab frame velocity, T is the ambient cell temperature, and m is the mass of CO_2 and tetrafluorobenzene, respectively. [d] Errors calculated with 95% confidence intervals. [e] The internal energy following 248 nm excitation of 1,2,3,4-tetrafluorobenzene is E'=41,274 cm^{-1}, 1,2,3,5-tetrafluorobenzene is E'=41,403 cm^{-1}, and 1,2,4,5-tetrafluorobenzene is E'=41,395 cm^{-1}, where differences are due to different amounts of thermal energy which are a result of differing vibrational frequencies. [f] The final CO_2 rotational energy state following collision with vibrationally excited donor.

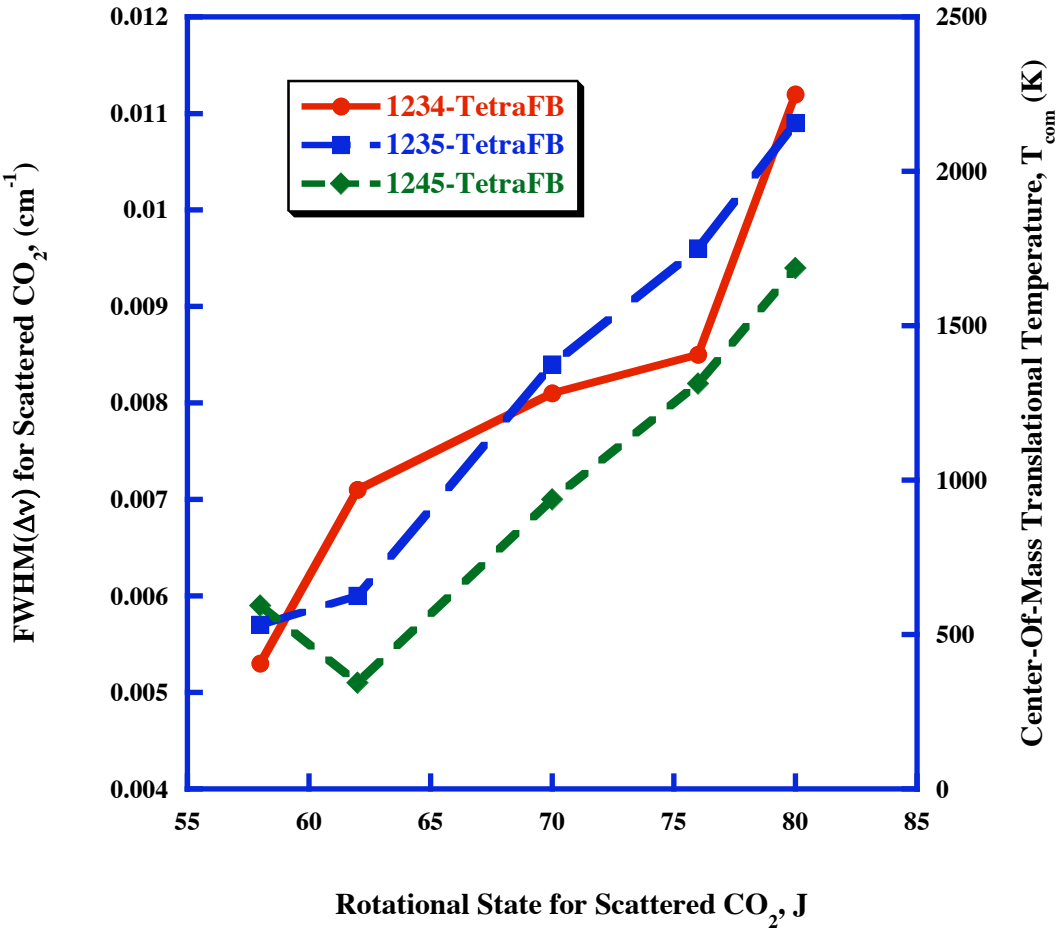

Figure 2.4: The FWHM Doppler linewidth of absorption transitions probing high rotational states (J=58-80) of CO_2 following collisions with vibrationally hot 1,2,3,5- TetraFB (blue), 1,2,4,5-TetraFB (green) and 1,2,3,4-TetraFB (red) is plotted against the final rotational state J. The linewidth in wavenumbers is plotted on the left axis and center of mass translational temperatures determined from the measured linewidths are given on the right y-axis. The linewidths are measured 1 μsec following 248 nm excimer laser excitation of the TetraFB, insuring that the measured velocity distributions are the result of single collisions between CO_2 and TetraFB ($\tau_{coll} \approx 4$ μsec). Plot shows that T_{com} increases monotonically with final J state.

wavenumbers. An upward trend between increasing J state and translational temperature for scattered CO_2 indicates higher J states have a larger distribution of translational temperature than scattering into lower states. The linear relationship is the result of a constant impact parameter over these J-states.[26] When comparing the plots for each of the molecules and taking into account the errors listed in the table, the similarity between each of the TetraFB isomers continues to be exhibited.

2.3.2 State-Resolved Scattering Energy Transfer Rate Constants and Probabilities.

Rate constants for scattering into each state are calculated at 1 μsec, much less than the mean gas kinetic collision time and thus represent the rate and probabilities of single collision events. The expression

$$k_2^J = \frac{\left[CO_2(00^00J,V)\right]}{\left[CO_2\right]_0\left[TetraFB^{E'}\right]_0 t} \tag{2.1}$$

is used to calculate this rate constant where $[CO_2\ (00^00J,V)]$ is the concentration of CO_2 molecules excited into a specific state obtained through infrared absorption measurements, $[CO_2]_0$ is the initial number of CO_2 molecules obtained through pressure, and $[TetraFB^{E'}]_0$ is the number of TetraFB molecules excited to energy E´ found through absorption of excimer laser pulses. Rate constants from collisions between hot (E´ ≈ 41,000 cm^{-1}) TetraFB with CO_2 are given in Table 2.2. To account for UV divergence, rate constants are scaled using the method described in the experimental section where experimental rate constants using pyrazine/CO_2 are scaled to literature values[20] and the same scaling is then applied to these rate constants. Table 2.2 also contains energy transfer probabilities representing the probability of a CO_2 molecule being scattered into a particular J state following a collision with TetraFB. These values are obtained using the relationship

Table 2.2: State-specific energy transfer rate constants $\left(k_2^J\right)$ and probabilities[a] $\left(k_2^J/k_{LJ}\right)$ for the energy transfer process tetrafluorobenzene$^{E'}$ + $CO_2(00^00)$→tetrafluorobenzene^{E} + $CO_2(00^00,J,V)$.

J_{final}	k_2^J (10^{-12} cm^3 molecule^{-1}s^{-1})		
	1,2,3,4-TetraFB	1,2,3,5-TetraFB	1,2,4,5-TetraFB
58	7.27±0.7	7.36±0.6	7.49±0.9
62	6.95±1.3	5.86±0.4	4.86±0.5
70	3.81±0.5	3.64±0.6	2.90±0.3
76	2.04±0.1	2.11±0.2	1.67±0.2
80	1.84±0.1	1.54±0.1	1.43±0.3
J_{final}	k_2^J/k_{LJ} (10^{-3})		
58	14.1±1	14.3±2.6	14.5±1.8
62	13.5±3	11.4±1.9	9.4±0.1
70	7.4±2	7.1±2.8	5.6±0.6
76	3.9±0.3	4.1±0.7	3.2±0.3
80	3.6±0.3	3.0±0.5	2.8±0.6

Table 2.2 continued

[a] The probability for energy transfer is given as $Prob_{LJ} = k_2^J/k_{LJ}$, where k_{LJ} is the Lennard-Jones has kinetic collision rate constant. It is defined (see Ref. 29) as $k_{LJ} = \pi\left[\left(d_{CO_2} + d_{tetrafluorobenzene}\right)/2\right]^2 \sqrt{\left(8k_BT\right)/\left(\pi\mu\right)}\Omega_{12}$, where d_{CO_2} = 4.5Å, Ref. 30, $d_{tetrafluorobenzene}$ = 5.4 Å (assumed to be equal to benzene, Ref. 30), k_B is Boltzmann's constant, and μ is the reduced mass. Ω_{12} is the Lennard-Jones collision integral given by the following expression:[31] $\Omega_{12} = \left[0.636 + 0.567\log(kT/\varepsilon_{12})\right]^{-1}$, where ε_{12} is tetrafluorobenzene-CO_2 well depth with ε_{CO_2}/k =195 K, (Ref.[30]), $\varepsilon_{1,2,3,4TetraFB}/k$=423 K, $\varepsilon_{1,2,3,5TetraFB}/k$=410 K, and $\varepsilon_{1,2,4,5TetraFB}/k$=418 K (Ref. 32), and $\varepsilon_{12} = \sqrt{\varepsilon_{CO_2}\varepsilon_{tetrafluorobenzene}}$. The Lennard-Jones collision rate constants at 298 K for the three isomers of tetrafluorobenzene are $k_{LJ(1,2,3,4TetraFB)} = 5.17\times10^{-10}$, $k_{LJ(1,2,3,5TetraFB)} = 5.14\times10^{-10}$, and $k_{LJ(1,2,4,5TetraFB)} = 5.16\times10^{-10}$ cm^3 $molecule^{-1}$ s^{-1}.

$$\text{Prob}^J = \frac{k_2^J}{k_{LJ}} \tag{2.2}$$

where the experimental rate constant is divided by the Lennard-Jones rate constant. Although Lennard-Jones almost certainly does not give an accurate description of the intermolecular potential, using it as a theoretical collision rate constant provides the benefit of allowing these results to be compared to those of previous studies and also compared within the group. A detailed discussion[14] of using Lennard-Jones as a scaling factor of energy transfer probability has been given elsewhere.

2.3.3 Energy Transfer Probability Distribution Function

The rate constants and energy transfer probabilities obtained in this study are indexed according to CO_2 rotational states; energy transfer probability can be resorted as a function of E − E′ to obtain *P(E,E′)*[5] where E′ is the precollision energy of the donor and E is the final energy of the donor following a single collision between donor and bath. Figure 2.5 plots *P(E,E′)* vs. ΔE using a linear scale for the y-axis. Previous work[5,6,12-14] has shown that a single exponential function is not sufficient to adequately describe the relationship between probabilities and their corresponding energy transfers given the constraints of normalization and detailed balance; therefore, a normalized double exponential function, including weak and strong collision parameters, developed by Troe[19] that fits the data with greater accuracy given the constraints has been used. Figure 2.6 displays both the experimental *P(E,E′)* and the fit of the double exponential function with a logarithmic scaled y-axis. The downward collision probabilities are described by the bi-exponential function according to

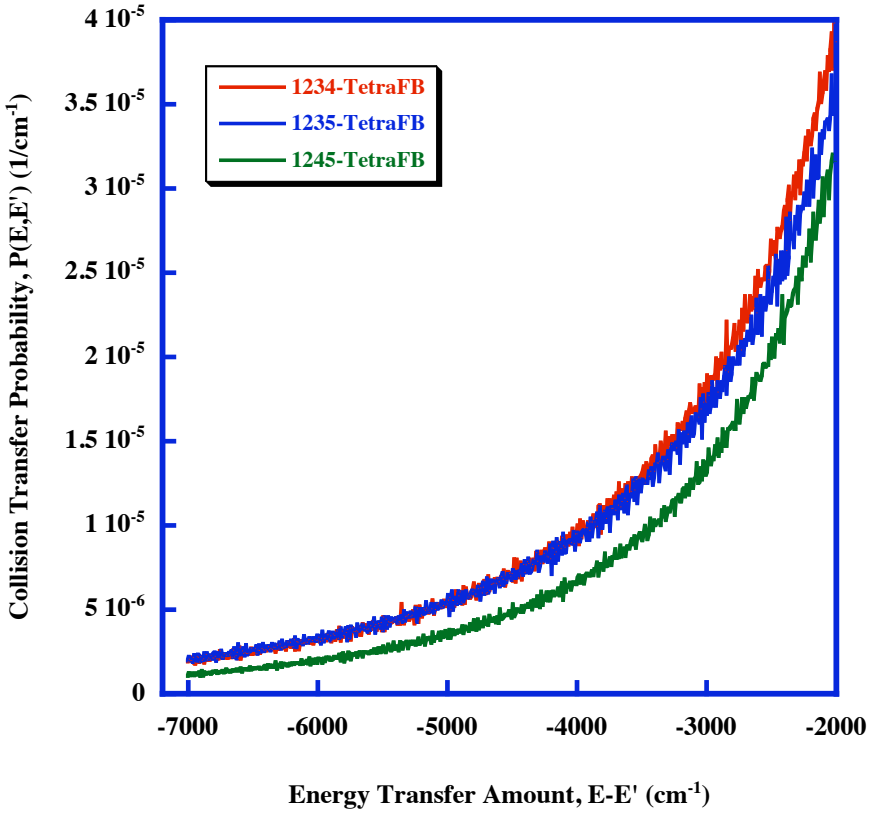

Figure 2.5: Shown are plots of the large ΔE tail of the energy transfer probability distribution function, P(E,E') describing the first Lennard-Jones collision between vibrationally excited 1,2,3,5- TetraFB (blue), 1,2,4,5-TetraFB (green) ,1,2,3,4-TetraFB (red) and C_6F_6(black) at energy E' ≈ 41,000 cm^{-1} and a CO_2 bath molecule resulting in CO_2 excitation into high rotational angular momentum states (J = 58 - 80) of the ground vibrational level.

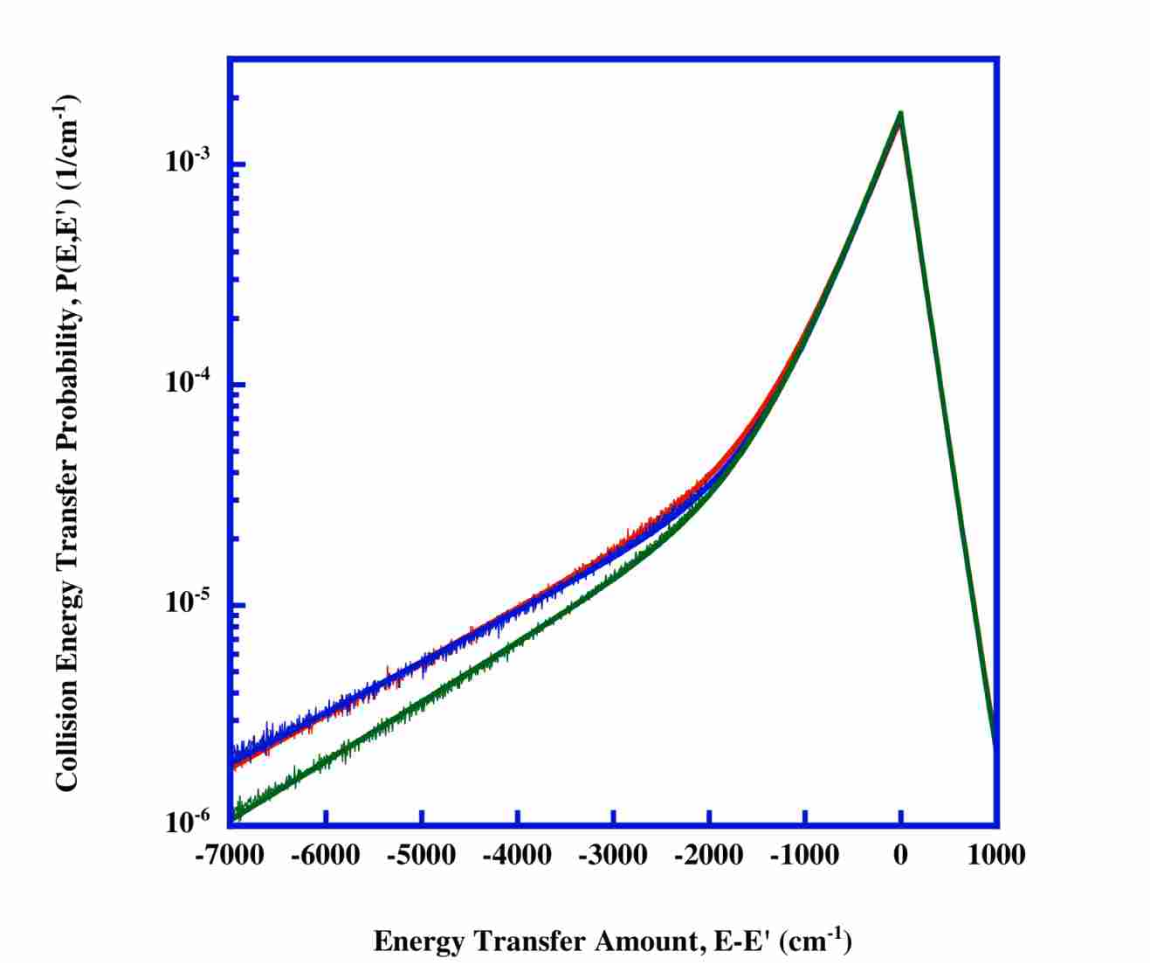

Figure 2.6: Plot (noisy line) of P(E, E') for 1,2,3,5- TetraFB (blue), 1,2,4,5-TetraFB (green) and 1,2,3,4-TetraFB (red) with CO_2 and E' ≈ 41,000 cm^{-1} along with the best-fit biexponential model functions (eq 2.3) (solid line). The P(E,E') shown is calculated based on the estimated value of $\langle J_i \rangle$=28.7 for the mean initial rotational state, J_i, for collisions populating high J_f states (J_f = 58 - 80) of CO_2.

$$P(E,E') = \frac{(1-f)\exp\{-(E'-E)/\alpha\} + f\exp\{-(E'-E)/\gamma\}}{(1-f)(\alpha+\beta) + f(\gamma+\delta)} \qquad E \le E' \tag{2.3}$$

The characteristic energy for downward "weak" collisions is represented by α, while downward "strong" (or super) collisions is given by γ. Upward collisions are given by the parameters β and δ for the respective weak and strong collisions where β and δ are related to α and γ by detailed balance.[19] The parameter *f* is related to the "fraction" of strong collisions; although not strictly a fraction, it does grow larger as the number of supercollision events increase. Another equation relating upward collisions is similar in form, but exchanges E for E′, α for β, and γ for δ. Fitting this function is not required since detailed balance is used to obtain up collision parameters from the fitted down collision parameters.

2.4 Discussion

The purpose of this study is to explore how molecular properties of the three TetraFB isomers correlate with their energy transfer probability distribution functions. The study is part of a larger systematic study of single collisions between CO_2 and the set of fluorinated benzene molecules. The study benefits from maintaining all experimental conditions while only changing the donor molecule. By looking at all of the fluorobenzenes, differences in the nature of energy transfer as a result of the number of flourines can be observed, as well as assessing the influence of changing the fluorine position within an isomer group. These changes alter various properties that have been linked to energy transfer efficiency. These include, but are not limited to, density of states, dipole moment, and frequency of specific vibrational modes, the latter which has been shown to be

particularly important. The set of fluorobenzene molecules provides twelve different donor molecules with the same number of vibrational modes, each with the same basic motion, varying only in frequency.

Beginning with a comparison of probabilities in Table 2.2 reveals that energy transfer probability of 1234-TetraFB and 1235-TetraFB are consistent with each other especially when experimental error is considered. Collisions between 1245-TetraFB and CO_2 result in consistently lower probabilities over a majority of the probed J states. It is no surprise then that the calculation of the probability distribution as ordered by energy transfer probability follows the same pattern over the range of ΔE=2000-7000 cm^{-1}. Comparison of *P(E,E')* (see Figure 2.5) shows similar red and blue lines representing 1234-TetraFB and 1235-TetraFB, but a lower green line representing 1245-TetraFB. C_6F_6 is also plotted in black as a reference and to assist in the fractional mode analysis.

Probability of energy transfer is linked to both the frequency of a mode and the fraction of molecules with sufficient energy in that mode to facilitate energy transfer[12,14,21] Considering only the frequency of vibration is a limited view of the overall picture. Clary and coworkers performed quantum scattering calculations[22] between benzene and helium to show that vibrational modes with lower frequency or out-of-plane motion were most responsible for energy transfer. This result was later confirmed through classical trajectory calculations[23] performed on CS_2. These studies indicated that lower frequency or out-of-plane motion had larger energy transfer cross sections allowing them to more efficiently transfer larger amounts of energy in a single collision. Clary[22] used the quantum scattering calculations to identify modes ν_6, ν_{11} and ν_{16} as those most responsible for energy transfer in collisions and as having the largest cross-section for energy transfer. The study went on

to show that in addition to frequency of vibration, the actual motion mattered as well. When ν_6, a stretching mode, was given the same frequency as ν_{16}, an out-of-plane bending mode, ν_{16} still had a larger energy transfer cross-section thus resulting in greater single energy transfer events. Lendvay[23] refers to these modes where large amounts of energy are leaked out as gateway modes.

A vibrational mode with a larger mass vibrates at a lower frequency and according to the calculations discussed above transfers more energy through a collision making it a more efficient mode at transferring energy, but the fraction of molecules with the necessary amount of energy required for a given ΔE must also be considered. Previous work[12] has shown that a "fractional energy transfer distribution" model or $f(E,E')$ relates the efficiency of a mode with the fraction of molecules having sufficient energy in that mode to transfer a particular ΔE. Because the molecules are not from the same point group, Wilson notation[33] is used for the comparison of vibrational frequencies. Wilson notation assigns vibrational modes based on motion of benzene-like molecules such that ν_1 is the same motion in every molecule irrespective of the molecule's point group. Because the assignment describes the same motion for all fluorinated benzene molecules, comparison of a mode is effectively a comparison of frequency.

Fractional mode analysis calculates the fraction of molecules within each mode that has sufficient energy to transfer and may shed light on which modes are responsible for energy transfer. Figure 2.7 gives a visual idea of how mode fractions for a molecule with a certain amount of energy change relative to each other. Three plots are shown in Figure 2.7 representing the fraction of modes with at least (a) 2000, (b) 5000, and (c) 8000 cm^{-1} of energy for all the TetraFB isomers and C_6F_6. Along the bottom of each plot are modes that

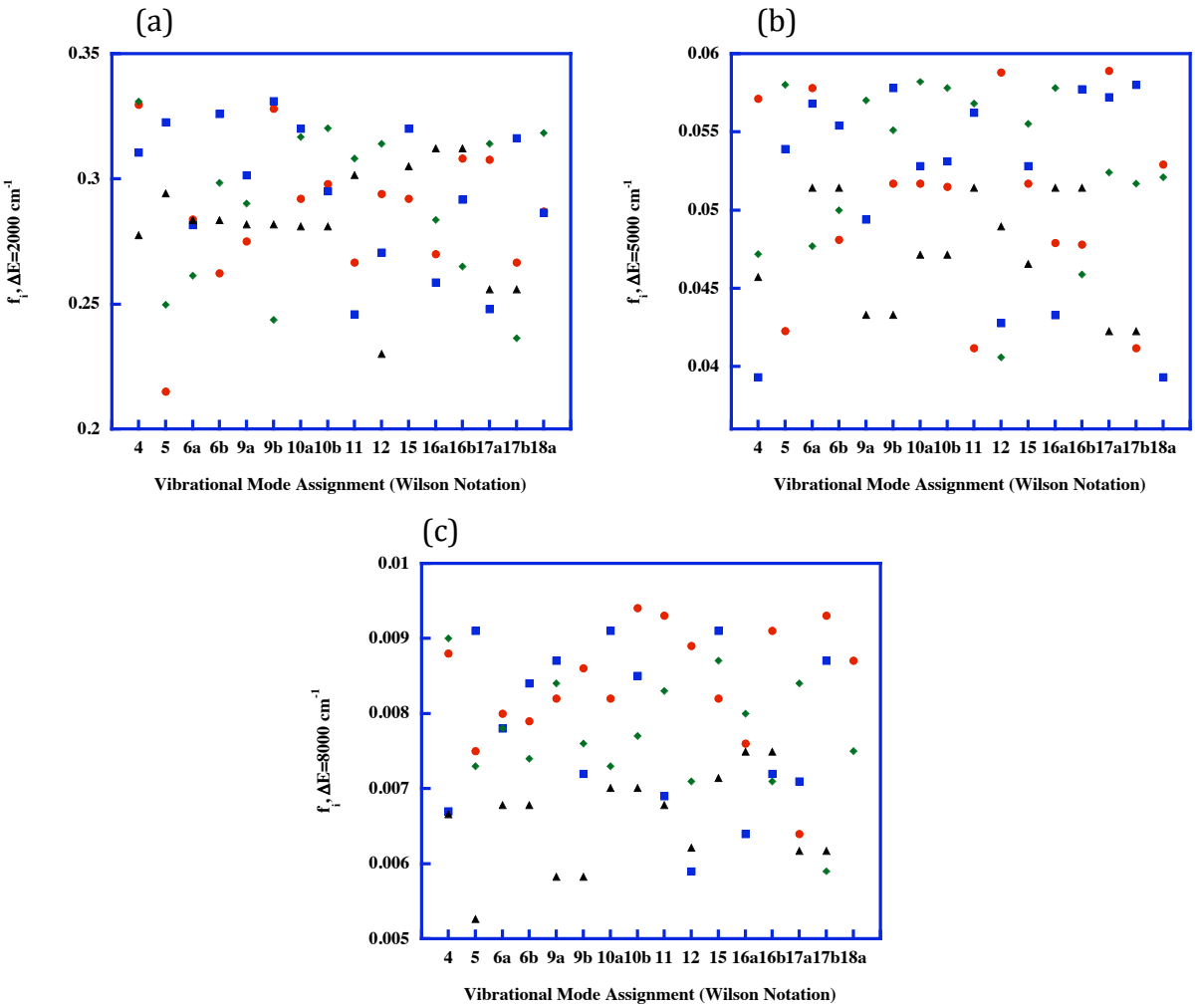

Figure 2.7: Fractional mode populations for highly vibrationally excited (E'~41,000 cm^{-1}) 1,2,3,4-TetraFB (red), 1,2,3,5-TetraFB (blue), 1,2,4,5-TetraFB (green) and C_6F_6 (black) with at least (a) 2000 cm^{-1}, (b) 5000 cm^{-1} and (c) 8000 cm^{-1}. The x-axis is the vibrational mode assignment according to Wilson notation, which has been used so that mode assignments represent the same vibrational motion in each molecule. Only the vibrational modes that were determined to be "gateway" energy transfer modes in quantum scattering calculation of the relaxation of benzene by He (ν_{6a}, ν_{6b}, ν_{11}, ν_{16a}, and ν_{16b}), the remaining out-of-plane or low frequency (<500 cm^{-1}) vibrational modes (ν_4, ν_5, ν_{10a}, ν_{10b}, ν_{17a}, ν_{17a}, and ν_{18b}) are also included in the figure.

are either low frequency (<500 cm^{-1}) or out-of-plane, as these modes, according to theory, are most likely to be responsible for the shape of *P(E,E')*; the y-axis shows the fraction of molecules for each mode that has at least the set amount of energy. Table 2.3 lists the frequencies of these vibrational modes for 1234-TetraFB, 1235-TetraFB, 1245-TetraFB, and C_6F_6 and indicates the modes whose motion is out-of-plane. Clary, *et al* have shown ν_{16} and ν_{11} of benzene to have greater energy transfer efficiencies and therefore have a larger influence on *P(E,E')*. By applying Clary's findings to the molecules in this study, ν_{16} and ν_{11} are the only modes that have C_6F_6 with a large fraction of molecules with at least 2000 cm^{-1} of energy and then a relative decrease in fraction as molecules with at least 5000 and 8000 cm^{-1} are considered. 1234 and 1235-TetraFB appear to also follow the trend especially when considering the frequency of vibration is lower for 1234-TetraFB in these modes of interest resulting in a slightly larger efficiency. 1245-TetraFB has the lowest probability for transferring energy over the magnitude of ΔE values according to the *P(E,E')* plot and yet has a largest fraction of molecules with energies 2000, 5000, and 8000 cm^{-1} relative to the fraction of other molecules considered in modes ν_{16} and ν_{11}. This apparent anomaly suggests 1245-TetraFB either does not use ν_{16} or ν_{11} as an energy transfer gateway or the model does not account for other possible sources of inefficiencies. One possible source could be large inefficiencies in other modes resulting in a lower overall magnitude for *P(E,E')*. The fraction only gives information about the number of molecules with that motion that have sufficient energy to transfer and relative mode efficiency based on frequencies can only be estimated. 1245-TetraFB has a consistently large fraction in modes ν_{16} and ν_{11} and a consistently lower magnitude in the *P(E,E')* relative to the other TetraFBs. This observation would suggest that if ν_{16} and ν_{11} are the energy transfer gateways, then

Table 2.3 The motion assignment of fundamental vibrational modes with frequency < 500 cm^{-1} for tetrafluorobenzene and C_6F_6.

Mode[a]	1,2,3,4-TFB[b]	1,2,3,5-TFB	1,2,4,5-TFB	C_6F_6	motion
4	169	706	669	249	o, ring deform
5	929	205	835	714	o, C-F bending
6a	459	458	485	264	ring stretching
6b	487	508	438	264	ring deform
9a	1175	310	280	443	C-F bending
9b	291	334	637	443	C-F bending
10a	374	258	417	370	o, C-F bending
10b	276	368	295	370	o, C-F bending
11	802	843	194	215	o, C-F bending
12	279	787	700	640	ring deform
15	748	258	299	208	C-F bending
16a	537	557	600	175	o, ring wagging
16b	596	610	456	175	o, ring wagging
17a	717	838	140	595	o, C-F bending
17b	802	139	867	595	o, C-F bending
18a	325	1130	346	1530	C-F bending
Tot. #	8	8	10	13	

Table 2.3 continued

o : out-of-plane motion

a : Wilson notation expression for fundamental vibrational mode[33]

b : Motion assignment for tetrafluorobenzene is obtained from Ref. 34 and 35

c : Motion assignment for perfluorobenzene is obtained from Ref. 36

1245-TetraFB must have a lower overall efficiency within all the modes in comparison to the other molecules. This explanation could account for the observation in ν_{16a}, but ν_{11} has a frequency four times smaller in 1245-TetraFB than the frequency of the other two. This low frequency should then have a much larger efficiency contributing greatly to the magnitude of *P(E,E')*.

Comparing the TetraFB set of isomers against other molecules of similar type requires several properties to be considered. Table 2.4 presents parameters obtained through fitting the experimental *P(E,E')* to the double exponential represented by eq 2.3 to *P(E,E')* for the three isomers of TetraFB along with values obtained from studies of C_6F_6,[5] the three DFB isomers,[13] and MFB.[37] The table also lists molecular properties of initial energy, dipole moment, density of states, and number of low frequency modes for each of the molecules. A similar initial energy among the fluorinated benzene molecules is advantageous and offers more consistency for comparison.

The first property to consider among all these molecules is the number of low frequency modes; these increase with the addition of more fluorines as would be expected. Previous work[14] suggested that the fraction of strong collisions, *f*, is linked to the number of low frequency modes. Among the TetraFBs, 1245-TetraFB would be expected to have a much different *f* due to the increase in low frequency modes, however the cutoff point used must also be taken into consideration. 500 cm^{-1} is arbitrarily chosen. If 600 cm^{-1} were chosen both 1235-TetraFB and 1245-TetraFB would have 11 low frequency modes, and at 400 cm^{-1} 1234-TetraFB and 1245-TetraFB would have 6 while 1235-TetraFB would have 7. An observation of similar *f* values between the three is not surprising. It would be

Table 2.4: The downward collision bi-exponential fit parameters (γ^a, α^b, f^c, and $\langle \Delta E \rangle_d{}^d$) for the experimentally obtained large delta E of *P(E,E')* in the high ΔE tail as well as several molecular parameters comprising initial energy E′, molecular dipole moments, the pre-collision state density, and the number of vibrational modes with frequency less than 500 cm^{-1} for various fluorinated benzene donors.

Donor	γ^a (cm^{-1})	α^b (cm^{-1})	f^c	$\langle \Delta E \rangle_d{}^d$ (cm^{-1})	Initial Energy, E′ (cm^{-1})	Dipole moment[e] (D)	ρ(E′)[f]	s < 500 cm^{-1} [g]
C_6H_5F[h]	1924	298	0.03	574	40,843	1.66	2.9×10^{16}	4
12-DFB[h]	1850	343	0.06	739	41,025	2.59	5.7×10^{17}	5
13-DFB[h]	2061	295	0.03	638	41,011	1.51	5.2×10^{17}	5
14-DFB[h]	2408	294	0.03	713	41,019	0	5.5×10^{17}	6
1234-TetraFB	1796	391	0.06	688	41,274	2.42	4.7×10^{19}	8
1235-TetraFB	1886	376	0.05	672	41,403	1.46	2.7×10^{20}	8
1245-TetraFB	1617	380	0.05	594	41,395	0	2.3×10^{20}	10
C_6F_6[h]	1411	620	0.15	847	41,822	0	2.1×10^{23}	13

Table 2.4 continued

[a] The characteristic strong energy transfer magnitude as determined from the biexponential fit of the *P(E,E')* data. [b] The characteristic weak energy transfer magnitude as determined from the biexponential fit of the *P(E,E')* data. [c] The "fraction" of strong collisions as determined from the biexponential fit of the *P(E,E')* data. [d] The average energy transferred in a single downward collision involving a vibrationally excited donor and CO2. Determined using the biexponential fit paramters according to $\langle \Delta E \rangle_d = (\alpha^2(1-x) + \gamma^2 x)/(\alpha(1-x) + \gamma x)$. [e] Molecular dipole moments obtained from ref 38. [f] The vibrational density of states for the donor molecule at the energy following the absorption of a 248 nm photon calculated using the Whitten—Rabinovitch algorithm (ref 39). [g] The number of vibrational normal modes with frequencies less than 500 cm^{-1}. Normal-mode frequencies for C_6F_6 are from refs 34 and 40 and 1,2,3,4-, 1,2,3,5- and 1,2,4,5-TetraFB are obtained from refs, 34 and 35. [h] *P(E,E')* parameters for MFB, DFB, and C_6F_6 are obtained from ref 5,13,37.

expected that the TetraFB isomers would have an *f* value that is closer to C_6F_6 than any of the DFB isomers, but 12-DFB is as large or larger than all of the TetraFB isomers. According to these results, the number of low frequency modes is not adequate to predict the difference *f* among the TetraFB isomers.

In addition to the number of low frequency modes, dipole moments have also been suggested to have an effect on energy transfer and ultimately *P(E,E')*. Mullin et *al.*[18] presented work comparing pyridine to pyrazine. They found pyridine to have a larger V→V energy transfer pathway relative to the V → RT in comparison to the ΔE pathways of pyrazine. The observation was attributed to the large (2.2 D) dipole moment of pyridine. Our lab experimentally determined *P(E,E')* for pyridine only to find that the fraction was much smaller in comparison to other molecules leading to the conclusion that dipole moment decreases the *P(E,E')* strong collision tail.[14]

The study presented here has the benefit of comparing three molecules of the same mass and elements that differ in dipole moment. The fraction of strong collisions may be connected to dipole moments; 1234-TetraFB and 12-DFB each have a dipole moment of around 2.5 D making them the most polar molecule in their respective isomer groups. These two polar molecules also share a value of 0.6 for the fraction of strong collisions, which is the largest fraction for those two groups. This correlation is not conclusive as of yet; an analysis of the TriFB isomers, currently underway, may provide more data to improve this observation. A comparison of the rotational temperatures of CO_2 following collisions with either DFB or TetraFB shows an opposing trend for DFB where the dipole moment increases while rotational temperature decreases; however, a direct trend is observed for TetraFB where increasing dipole also increases rotational temperature. This

observation may be more related to mass distribution than actual dipole moment or may not have any real correlation A study of the V → V energy transfer pathway for these two groups could shed new light on this apparent phenomenon.

Scientists[13,14,21,41-44] are beginning to establish a correlation between the shape of the energy dependent density of states and *P(E,E′)* through multiple studies and the TetraFB study is no exception. The basis of the model comes through the following equation, which is an application of Fermi's Golden rule

$$P(E,E') \propto \left|V_{if}\right|^2 \rho(E)\rho(E') \tag{2.4}$$

where V_{if} represents the matrix element, $\langle i \left| H \right| f \rangle$, which couples initial and final states, and $\rho(E)$ and $\rho(E')$ are the density of states at E and E' respectively. Figure 2.8 plots the shape of *P(E,E′)*, represented by the values of the inverse of gamma and alpha, against the energy dependent state density given by the slope of $\ln[\rho(E'-\Delta E)]$ versus ΔE. Several molecules are represented in the plot; from left to right they are MFB, 3 DFB isomers, 3 TetraFB isomers, and C_6F_6. Tetra FB shows good correlation for both the inverse of alpha, the weak collision fitting parameter, as well as for the inverse of gamma, the strong collision fitting parameter. The strong correlation with the inverse of gamma can be attributed to the experimental measurement of the large ΔE portion of *P(E,E′)*. The inverse of alpha shows only a reasonably good linear fit. Errors are expected given that the small ΔE portion of *P(E,E′)* is based on an extrapolation of the experimental portion of *P(E,E′)* using eq 2.3 and therefore introduce greater uncertainty in the small ΔE region. With that said, the isomers of TetraFB show a strong fit to this linear relationship for both alpha and gamma despite the introduction of any error resulting from extrapolation. The graph clearly shows that the

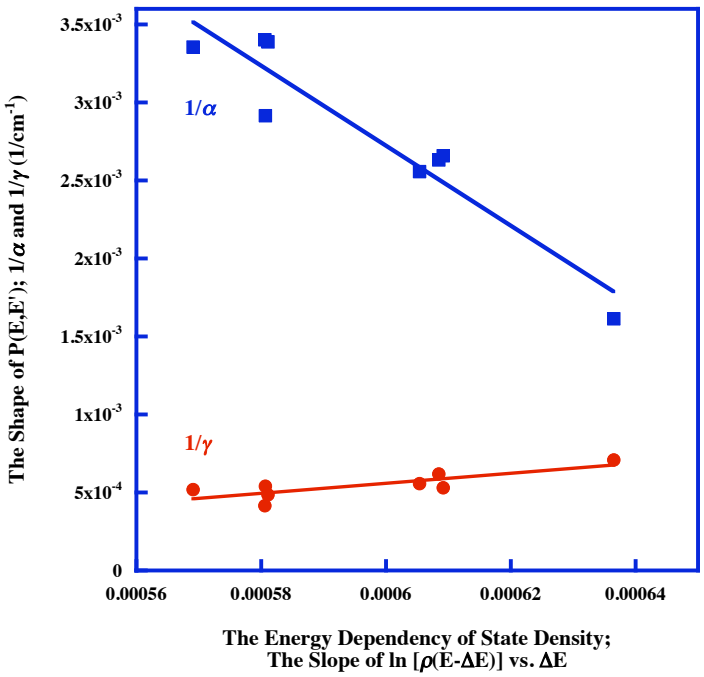

Figure 2.8: The correlation between the shape of P(E,E') as determined by the biexponential fit parameters ($1/\alpha$ and $1/\gamma$) and the shape of energy dependent state density of the donor molecules given by the slope of $\ln[\rho(E'-\Delta E)$ vs ΔE. Circles represent the characteristic energy transfer magnitude for "strong" collisions (γ) while the squares are the characteristic energy transfer magnitude for "weak" collisions (α). Based on the application of Fermi's Golden Rule to collisional deactivation of vibrationally excited donor molecules in collisions with CO_2. From left to right in the figure data points are for monofluorobenzene, the three difluorobenzenes, the three tetrafluorobenzenes, and C_6F_6. Monofluorobenzene, difluorobenzenes, and C_6F_6 data are from Refs (5,13,37). The shape of the energy transfer distribution function as a function of ΔE mirrors the shape of the final donor density of states as a function of energy transferred (ΔE). The shape of both the strong and weak collision region of P(E,E') is correlated with the donor molecule's final density of states.

density of states, which is a better way to represent the lowering of frequency over all modes, does effect the shape of P(E,E') and ultimately the amount of energy transferred in a collision.

2.5 Conclusion

The collisional relaxation of 1234-TetraFB, 1235-TetraFB, and 1245-TetraFB following collisions with CO_2 has been studied by probing CO_2 energy gain using transient IR diode laser spectroscopy. Rotational populations and recoil velocity distributions for rotational states J=58-80 of the 00^00 level of CO_2 were measured. Rate of scattering into these states was also measured and used to calculate state resolved energy probabilities that are resorted according to ΔE to give the large ΔE region of the energy transfer distribution function or *P(E,E')*. A double exponential function was used to fit this function giving parameters representing strong and weak collisions; these parameters were found to be largely dependent on the shape of the donor's state density plotted as a function of internal energy. Dipole moment has also been shown to have a possible correlation with the fraction of strong collisions, and fractional mode analysis has shown ν_{16} and ν_{11} as the most probable gateway modes for TetraFB.

2.6 References

1. Hinshelwood, C. N., *Proc. R. Soc. A* **1927,** *113*.

2. Lindemann, F. A., *Transactions of the Faraday Society* **1922,** *17*, 598-606.

3. Hippler, H.; Troe, J., Recent Direct Studies of Collisional Energy Transfer in Vibrationally Highly Excited Molecules in the Ground Electronic State. In *Bimolecular*

Collisions, Ashfold, M. N. R.; Baggott, J. E., Eds. Royal Society of Chemistry: London, 1989; pp 209-262.

4. Gilbert, R. G.; Smith, S. C., *Theory of Unimolecular and Recombination Reactions*. Blackwell Scientific Publications: Oxford, U. K., 1990.
5. Michaels, C. A.; Flynn, G. W., *Journal of Chemical Physics* **1997,** *106* (9), 3558-3566.
6. Michaels, C. A.; Lin, Z.; Mullin, A. S.; Tapalian, H. C.; Flynn, G. W., *Journal of Chemical Physics* **1996,** *106* (17), 7055-7071.
7. Lenzer, T.; Luther, K.; Reihs, K.; Symonds, A. C., *J. Chem. Phys.* **2000,** *112* (9), 4090-4110.
8. Toselli, B. M.; Brenner, J. D.; Yerram, M. L.; Chin, W. E.; King, K. D.; Barker, J. R., *J. Chem. Phys.* **1991,** *95* (1), 176-188.
9. Toselli, B. M.; Barker, J. R., *J. Chem. Phys.* **1992,** *97*, 1809-1817.
10. Luther, K.; Reihs, K., *Ber. Bunsenges. Phys. Chem.* **1988,** *92*, 442-445.
11. Flynn, G. W.; Weston, R. E., Jr., *Journal of Physical Chemistry* **1993,** *97* (31), 8116-8127.
12. Sevy, E. T.; Rubin, S. M.; Lin, Z.; Flynn, G. W., *Journal of Chemical Physics* **2000,** *113*, 4912-4932.
13. Mitchell, D. G.; Johnson, A. M.; Johnson, J. A.; Judd, K. A.; Kim, K.; Mayhew, M.; Powell, A. J.; Sevy, E. T., *Journal of Physical Chemistry A* **2008,** *112* (6), 1157-1167.
14. Johnson, J. A.; Kim, K.; Mayhew, M.; Mitchell, D. G.; Sevy, E. T., *Journal of Physical Chemistry A* **2008,** *112* (12), 2543-2552.
15. Li, Z.; Korobkova, E.; Werner, K.; Shum, L.; Mullin, A. S., *Journal of Chemical Physics* **2005,** *123* (17), 174306.

16. Havey, D. K.; Liu, Q.; Li, Z.; Elioff, M.; Fang, M.; Neudel, J.; Mullin, A. S., *Journal of Physical Chemistry A* **2007,** *111* (13), 2458-2460.

17. Havey, D. K.; Liu, Q.; Mullin, A. S., Energy transfer and reactivity of vibrationally hot aromatic moleucles with H_2O. In *232nd ACS National Meeting*, San Francisco, CA, 2006.

18. Wall, M. C.; Stewart, B. A.; Mullin, A. S., *Journal of Chemical Physics* **1998,** *108* (15), 6185-6196.

19. Troe, J., *J. Chem. Phys.* **1992,** *97*, 288-292.

20. Mullin, A. S.; Michaels, C. A.; Flynn, G. W., *Journal of Chemical Physics* **1995,** *102* (15), 6032-6045.

21. Johnson, J. A.; Duffin, A. M.; Hom, B. J.; Jackson, K. E.; Sevy, E. T., *Journal of Chemical Physics* **2008,** *128*, 054304.

22. Clary, D. C.; Gilbert, R. G.; Bernshtein, V.; Oref, I., *Faraday Discuss.* **1995,** *102*, 423-433.

23. Lendvay, G., *J. Phys. Chem. A* **1997,** *101* (49), 9217-9223.

24. Khan, F. A.; Kreutz, T. G.; Flynn, G. W.; Weston, R. E., Jr., *Journal of Chemical Physics* **1990,** *92*, 4876-4886.

25. Sevy, E. T. Ph.D. Dissertation. Columbia University, 1999.

26. Mullin, A. S.; Park, J.; Chou, J. Z.; Flynn, G. W.; Weston, R. E., Jr., *Chemical Physics* **1993,** *175*, 53-70.

27. Pugh, L. A.; Rao, K. N., Intensities from infrared spectra. In *Molecular Spectroscopy: Modern Research Volume II*, Rao, K. N., Ed. Academic Press: New York, 1976; pp 165-227.

28. Rothman, L. S.; Gamache, R. R.; Barbe, A.; Goldman, A.; Gillis, J. R.; Brown, L. R.; Toth, R. A.; Flaud, J. M.; Camy-Peyret, C., *App. Opt.* **1983,** *22*, 2247.

29. Smith, I. W. M., *Kinetics and Dynamics of Elementary Gas Reactions*. Butterworths: London, 1980.

30. Hirschfelder, J. O.; Curtiss, C. F.; Bird, R. B., *Molecular Theory of Gases and Liquids*. John Wiley & Sons, Inc.: New York, 1954.

31. Troe, J., *J. Chem. Phys.* **1977,** *66*, 4758-4775.

32. Lin, H. M.; Seaver, M.; Tang, K. Y.; Knight, A. E. W.; Parmenter, C. S., *Journal of Chemical Physics* **1979,** *70* (12), 5442-57.

33. Wilson, E. B., Jr., *Physical Review* **1934,** *45*, 706-14.

34. Eaton, V. J.; Steele, D., *J. Mol. Spec.* **1973,** *48*, 446-458.

35. Valerie J. Eaton, R. A. R. P., D Steele, and J W Tindle, *Spectrochimica Acta* **1976,** *32A*, 9.

36. Steele, D., *Spectrochimica Acta* **1962,** *18*, 915-25.

37. Kim, K.; Johnson, A. M.; Powell, A. L.; Mitchell, D. G.; Sevy, E. T., *Journal of Physical Chemistry A* **In Preparation**.

38. Doraiswamy, S.; Sharma, S. D., *Theochem* **1983,** *94* (1-2), 63-71.

39. Whitten, G. Z.; Rabinovitch, B. S., *J. Chem. Phys.* **1963,** *38* (10), 2466-2473.

40. Pearce, R. A. R.; Steele, D.; Radcliffe, K., *Journal of Molecular Structure* **1973,** *15*, 409-420.

41. Miller, E. M.; Murat, L.; Bennette, N.; Hayes, M.; Mullin, A. S., *Journal of Physical Chemistry A* **2006,** *110* (9), 3266-3272.

42. Park, J.; Li, Z.; Lemoff, A. S.; Rossi, C.; Elioff, M. S.; Mullin, A. S., *J. Phys. Chem. A* **2002,** *106*, 3642-3650.

43. Park, J.; Shum, L.; Lemoff, A. S.; Werner, K.; Mullin, A. S., *J. Chem. Phys.* **2002,** *117*, 5221-5233.

44. Elioff, M. S.; Fang, M.; Mullin, A. S., *Journal of Chemical Physics* **2001,** *115* (15), 6990-7001.

Chapter 3

Collisional Relaxation of the Three Vibrationally Excited Trifluorobenzene Isomers by Collisions with CO_2: Effect of Dipole Moment on Fraction of Strong Collisions

3.1 Introduction

Collisional energy transfer has intrigued scientists[1,2] for decades. In part, this interest is due to the close relationship between energy transfer and unimolecular reactions. This close relationship between energy transfer and unimolecular reactions can clearly be seen in master equation modeling of thermal unimolecular reactions.[3] A key component of the master equation is the rate at which energy is transferred to or from a molecule prior to product formation as contained in the energy transfer probability distribution function or *P(E,E′)*. *P(E,E′)* is the probability that a molecule with initial energy E′ will have energy E following a single collision. Although *P(E,E′)* has long been recognized as the key energy transfer kinetic measurement, it has only been in the past 10 years that experimental techniques have been capable of measuring *P(E,E′)* for large molecules with chemically significant amounts of energy. The first experimental measurements were made by Flynn and coworkers;[4,5] other techniques have since been used to measure *P(E,E′)* including KCSI[6-8] and molecular beam imaging techniques.[9-11] However, as experimental measurements are still relatively recent, correlation between molecular properties and the form of *P(E,E′)* are not well established. Efforts in our lab[12,13] have focused on making connections between *P(E,E′)* shape and molecular properties of collision partners.

Our lab uses experimental methods similar to those developed by Flynn[14,15] and used by the Mullin.[16,17] A donor molecule is electronically excited using an excitation laser; following a rapid radiationless relaxation into the ground electronic state, the now vibrationally hot donor molecule collides with a bath molecule transferring large amounts of energy to the bath. Energy transfer has been studied by observing energy loss from the donor, but when studying molecules with chemically significant amounts of energy, it is

only possible to measure the average amount of energy transferred. Because the amount of energy lost by the donor is equal to the energy gained by the bath, if simple bath molecules are chosen where individual ro-vibrational states can be probed by the diode laser, single collision energy transfer can be studied using this technique. Although vibrational energy is transferred to both the vibrational (V–V) and the rotational and translational (V–RT) degrees of freedom of the bath, our studies here focus on the V–RT pathway accounting for ~90% of the total energy transfer probability. This is accomplished through measuring the population of a selected ro-vibrational peak by measuring the absorption at the linecenter and the recoil velocity through a measure of the Doppler broadened lineshapes. Measuring these lineshapes is made possible because the laser frequency bandwidth (ν=0.0003 cm^{-1}) is considerably smaller than a CO_2 room temperature lineshape (ν=0.0042 cm^{-1}).[14,18] In addition to this, the rate of scattering into a selected ro-vibrational state is measured. These measurements can be used to obtain *P(E,E')* for a given donor-bath pair.

Knowing how *P(E,E')* compares graphically, based on experimental results, to other molecules is useful, but a few parameters that represent this function and have chemical meaning would allow for simpler comparisons. A double exponential function has been shown[3,19] to fit the shape of *P(E,E')* well. This function gives parameters related to the shape of *P(E,E')* and which represent the average energy of weak and strong collisions where energy is both gained and lost. The "up" collision, relative to donor, parameters are not necessary to directly measure as they are related to the down collision parameters via detailed balance. These parameters are useful when comparing how weak and strong collisions change based on the donor molecule in use. Ongoing research[13,15,20] has found density of states to largely influence these weak and strong parameters and thus the shape

of *P(E,E')*. One other useful parameter is generally referred to as the fraction of strong collisions and increases as the fraction of strong collisions increase. Previous work[21] has shown the number of low frequency modes (<500 cm^{-1}) to effect the fraction of strong collisions.

In addition to knowing *P(E,E')*, the modes that are most responsible for the shape of *P(E,E')* can also be determined. Sevy[15] presented the idea of a fractional energy transfer distribution or *f(E,E')* model that relates mode efficiency and fraction of molecules in the mode with sufficient energy to transfer. The function will closely mirror the shape of *P(E,E')* for the modes that are most involved in energy transfer. Clary[22] first suggested the idea of certain modes being responsible for a majority of the energy transfer through quantum scattering calculations using benzene and helium. He showed certain modes had larger energy transfer cross sections making them more likely to participate in a collision. The size of this cross section could be increased with lower frequency modes or out-of-plane motion causing these modes to be more efficient at transferring large amounts of energy. Lendvay[23] referred to these vibrational modes through which energy leaks out of the molecule as “gateway modes”.

This study joins with previous work performed by our lab to experimentally determine *P(E,E')* for all fluorinated benzene derivatives and make comparisons between the entire group. Here we present 1,2,3-trifluorobenzne, 1,2,4-trifluorobenzne, and 1,3,5-trifluorobenzne representing all the isomers of trifluorobenzene (TriFB). We will largely make comparisons between the TriFBs and previous fluorobenzene studies including monofluorobenzene (MFB),[24] the three diflurobenzene (DFB) isomers,[13] thee three tetraflurobenzene (TetraFB) isomers,[25] and C_6F_6.[5] Using this comprehensive group of

molecules, each has the same number of vibration modes with generally the same motion and differing in frequency; the chemical make-up is also similar along with internal energy. Comparisons between the isomers of TriFB allow for even more subtle changes to be considered; mass will not change nor will chemical make-up leaving only dipole moment and frequencies of motion as variables for comparison.

3.2 Experiment

The UV pump, IR probe technique used to study the collisional relaxation of the three isomers of trifluorobenzene has been described in detail elsewhere;[12] therefore, only a brief outline of the method is presented here. A 1:1 mixture of gas phase trifluorobenzene and CO_2 flows through a 3.0 m collision cell at a total pressure of ~20 mTorr. A 248 nm KrF excimer laser (Lamda Physik Complex 201) creates excited TriFB via the $S_1 \leftarrow S_0$ transition of trifluorobenzene. Electronically excited trifluorobenzene then undergoes a rapid radiationless internal conversion into high-vibrationally excited states in the ground electronic state, $S_1 \rightarrow S_0^*$. Energy gain into individual rotational states of CO_2 (00^00,J=58, 62, 70, 76, or 80) resulting from collisions with hot trifluorobenzene in S_0^* is monitored by probing the transient absorption of IR light (λ= 4.3 μm) that is collinearly propagated with the UV beam through the collision cell. The highly resolved (0.0003 cm^{-1}) IR laser (Laser Components) is used to probe the scattered CO_2 molecules via the antisymmetric stretch transition in CO_2. To insure that only a single diode laser mode is detected, the infrared light passes through a single grating monochromator (Acton Spectra pro 500i) before being focused onto a liquid nitrogen cooled InSb detector.

Two types of measurements are collected: the transient fractional absorption $\Delta I/I_0$, recording the value at 1 μs following each laser pulse (the mean collision time is 4 μs) and the full width at half max (FWHM) of each of the rotational states. From these two measurements, we determine the amount of energy gained by CO_2. A reference CO_2 signal is created by passing ~4% of the IR light through a CO_2 reference cell into a second monochromator and detector and stored on an oscilloscope. Rotational populations are measured by locking the frequency of the diode to the center of this CO_2 reference peak. The CO_2 translational energy gained is determined through the Doppler broadened linewidths of each rotational peak. For FWHM measurements, the entire ro-vibrational lineshape must be measured. This is done by collecting a transient signal at about 40 evenly spaced frequencies across the line. To adjust the frequency, the diode frequency is locked to a fringe of a scanning Fabry–Perot Etalon (free spectral range = 289 MHz); the frequency of the laser is known through a DAC calibration by which the etalon is scanned between two CO_2 peaks of known frequency, is changed. The measured lineshape is then fit to a Gaussian function to determine the FWHM. Rotational populations and recoil velocities were measured for peaks 58, 62, 70, 76, and 80 in our experiment.

Because of excimer laser divergence down the collision cell, rate constants are only relatively accurate; therefore, a calibration experiment was also performed[12] which scales experimentally obtained pyrazine rate constants with literature values.[20] That same scaling factor is then applied to a simultaneously measured trifluorobenzene rate constant allowing for consistent comparisons across all isomers and with other molecules.

The 1,2,3-triflurobenzene (Aldrich, 99% purity), 1,2,4-trifluorobenzene (Aldrich 98% purity) and 1,3,5-trifluorobenzene (97% purity) were purified prior to our experiments using the freeze-pump-thaw method.

3.3 Results

3.3.1 Rotational and Translational Excitation of Carbon Dioxide Bath.

Transient CO_2 populations of various rotational states between J=58 and 80 in the ground vibrational level(00^00) were measured using infrared absorption following 248nm UV excitation of 123-TriFB, 124-TriFB, and 135-TriFB. Transient absorption signals for the p70 {(00^01, J=69) ← (00^00, J=70)} CO_2 transition at 2279.8391 cm^{-1} resulting from collisions with each of the fluorinated benzenes investigated in this study are shown in Figure 3.1 as a function of time relative to the excimer laser pulse. The signals shown represent the average taken over 100 laser shots fired into a 1:1 flowing 20.0 mTorr gas mixture of CO_2 and triflurobenzene. Data at early times is dominated by scattering of CO_2 into the probe state by single collisions with excited TriFB[26] Following a laser pulse, CO_2 molecules are scattered into the state by collisions with the excited donor molecule. Data at times greater than 4 μsec become much more complicated as the state continues to be filled due to additional collisions with slightly thermalized TriFB molecules as well as CO_2 molecules in higher rotational states relaxing into the state being probed. The population at later times decreases simply through CO_2 molecules undergoing relaxation out of the high angular momentum states. The weak signal observed for 123 and 135-TriFB is due to limited absorption of the UV light at 248 nm for these two molecules. Measured

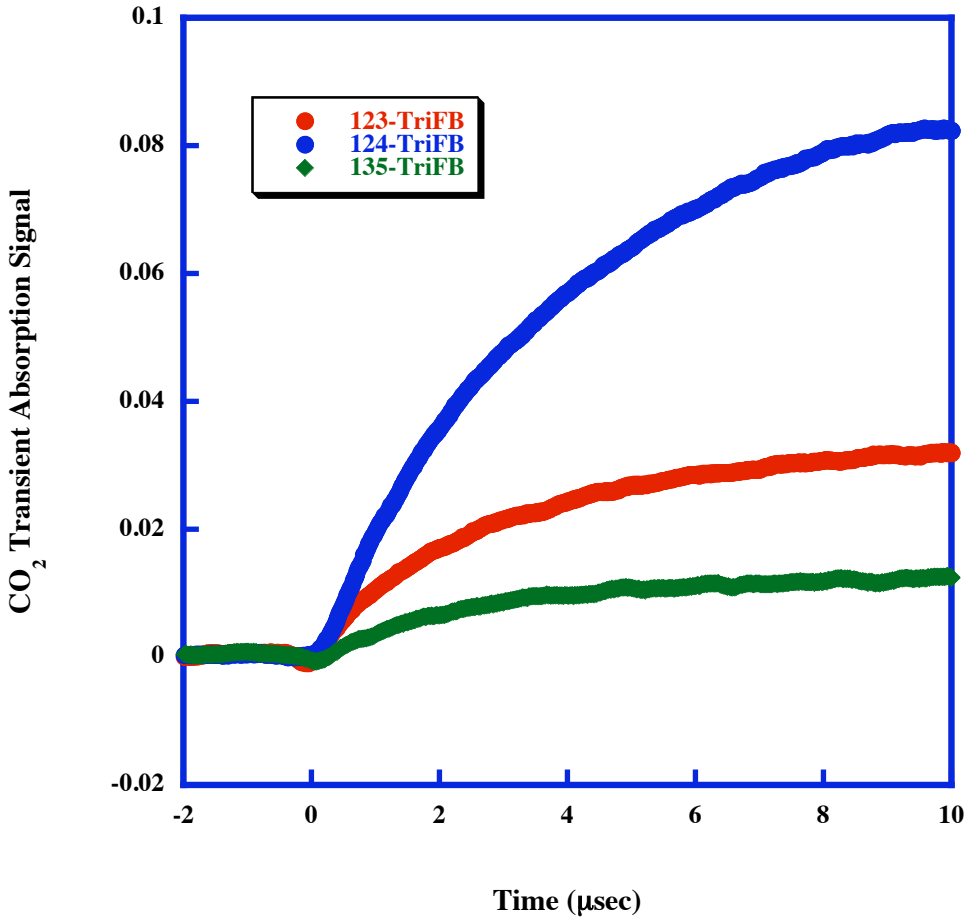

Figure 3.1: The fractional IR absorption of CO_2 collisionally scattered into the 00^00, J=70 state as a function of time following UV excitation of the three isomers of trifluorobenzene (TriFB). To ensure that the measured energy transfer parameters represent single collision events, transient signals are measured at 1 μsec (1/4 the mean collision time) following a laser pulse of a flowing gas mixture of 10 mtorr CO_2 and 10 mtorr of 1,2,3-TriFB (red), 1,2,4- TriFB (blue), or 1,3,5-TriFB (green).

absorptions are converted[27] to CO_2 number density using absorption line strengths found in the HITRAN spectroscopic database[28].

Figure 3.2 shows a Boltzmann plot of the rotational state distribution of CO_2 following a collision with TriFB. A linear relationship observed over this set of J states allows for a single temperature to describe each distribution. The temperatures obtained for CO_2 following collisions with 123-, 124- and 135-TriFB are 947 ± 43K, 920 ± 70K, 870 ± 110K, respectively. These values are consistent with rotational temperatures of high-J tails found in previous studies of other fluorinated benzene molecules. (C_6H_6: 795 K[5]; $C_6H_4F_2$: isomers 930, 970, and 1020 K[13]; $C_6H_2F_4$: isomers 940, 920, and 870 K). It is important to note that this distribution is not representative of all states; rather it describes the distribution over the states of the high-J tail and not necessarily of those in the low-J tail.

Doppler Broadened line shapes are measured to determine the velocity distribution of CO_2 molecules in each excited J state following collisions with TriFB. In Figure 3.3a, a Doppler broadened line shape for the p70 transition of CO_2 following a single collision with 123-TriFB is measured by averaging the transient signal at 1 μsec after the laser pulse for each of 40 different equally spaced frequencies across the CO_2 rovibrational transition. A Gaussian function most accurately fits the observed data; because of the Gaussian distribution, a single translational temperature, which is related to the full width at half maximum (FWHM), can accurately describe the distribution of CO_2 velocities. For the p70 transition shown in Fig 3a, FWHM of 0.0079 ± 0.0007 cm^{-1} was calculated from the Gaussian fitting parameters, which corresponds to a translational temperature of 1033K. Figures 3.3b and 3.3c represent lineshapes of the p70 transition for the reaction mixtures of 124-TriFB and 135-TriFB with CO_2, respectively, and give T_{trans} values of 1589 K

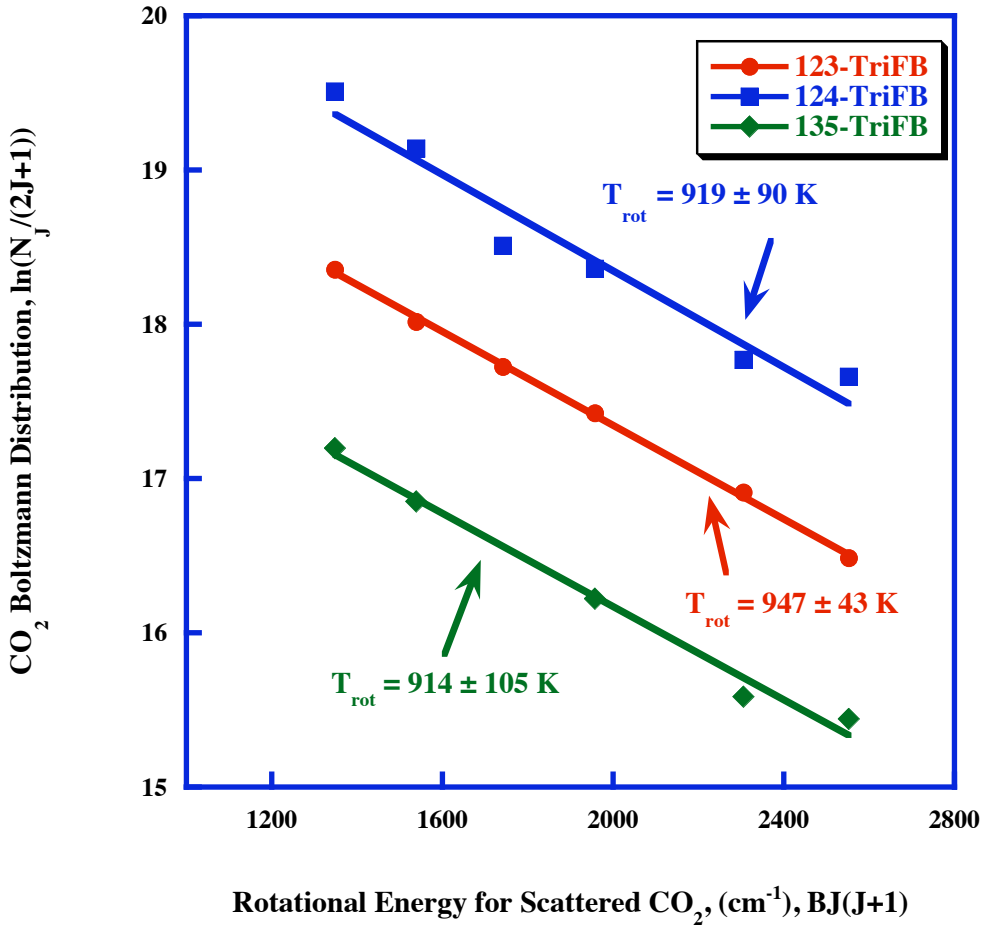

Figure 3.2: Boltzmann plot of the nascent rotational distributions in the ground vibrational level of CO_2 following excitation by single collisions with vibrationally hot 1,2,3- TriFB (red), 1,2,4-TriFB (blue) or 1,3,5-TriFB (green). Points are calculated from the factional absorption of CO_2 at 1 μsec after UV excitation of donor. The solid lines are the best linear least squares fit to the experimental points measured over the range J = 58 to 80. The slope of the best fit line is equal to $-1/k_B T_{rot}$ and the number densities, N(J), are in units of molecules/cm^3. The rotational temperature for CO_2 molecules scattered into the high J states following collisions with 1,2,3-, 1,2,4-, and 1,3,5-TriFB is 947 ± 43 K, 919 ± 90 K and 914 ± 105 K, respectively. Error represents 95% confidence limits.

Figure 3.3: Nascent Doppler broadened lineshapes for the absorption transition CO_2 (00^00; J=70) → CO_2 (00^01; J=69) obtained by probing CO_2 molecules excited by collisions with vibrationally excited (a) 1,2,3-, (b) 1,2,4- and (c) 1,3,5-TriFB. The lineshapes were obtained using a flowing mixture of 10 mTorr CO_2 and 10 mTorr TriFB. The points represent the fractional IR absorption of CO_2 collisionally scattered into the 00^00, J=70 state measured 1 μsec following 248 nm excimer laser pumping of TriFB. Absorption measurements are averaged over approximately 40 transient signals at each diode laser frequency across the line. The solid lines are the best non-linear least squares fit to a Gaussian function. The full width at half maximum (FWHM) obtained from the measured lineshapes is 0.0079 ± 0.0007, 0.0098 ± 0.0009, and 0.0082 ± 0.0011 cm^{-1} for 1,2,3-, 1,2,4-, and 1,3,5- TriFB, respectively. For comparison, the FWHM of a CO_2 lineshape with T_{trans} = 300 K is approximately 0.0042 cm^{-1}. The final translational temperature, T_{trans}, is related to the linewidth, $\Delta\nu_0$ (full width at half maximum) through the expression $T_{trans}(K)=[mc^2(\Delta\nu_{obs})^2]/[8Rln2(\nu_0)^2]$, where m is the mass of CO_2, c is the speed of light, R is the gas constant, and ν_0 is the wavenumber at the center of the absorption line.

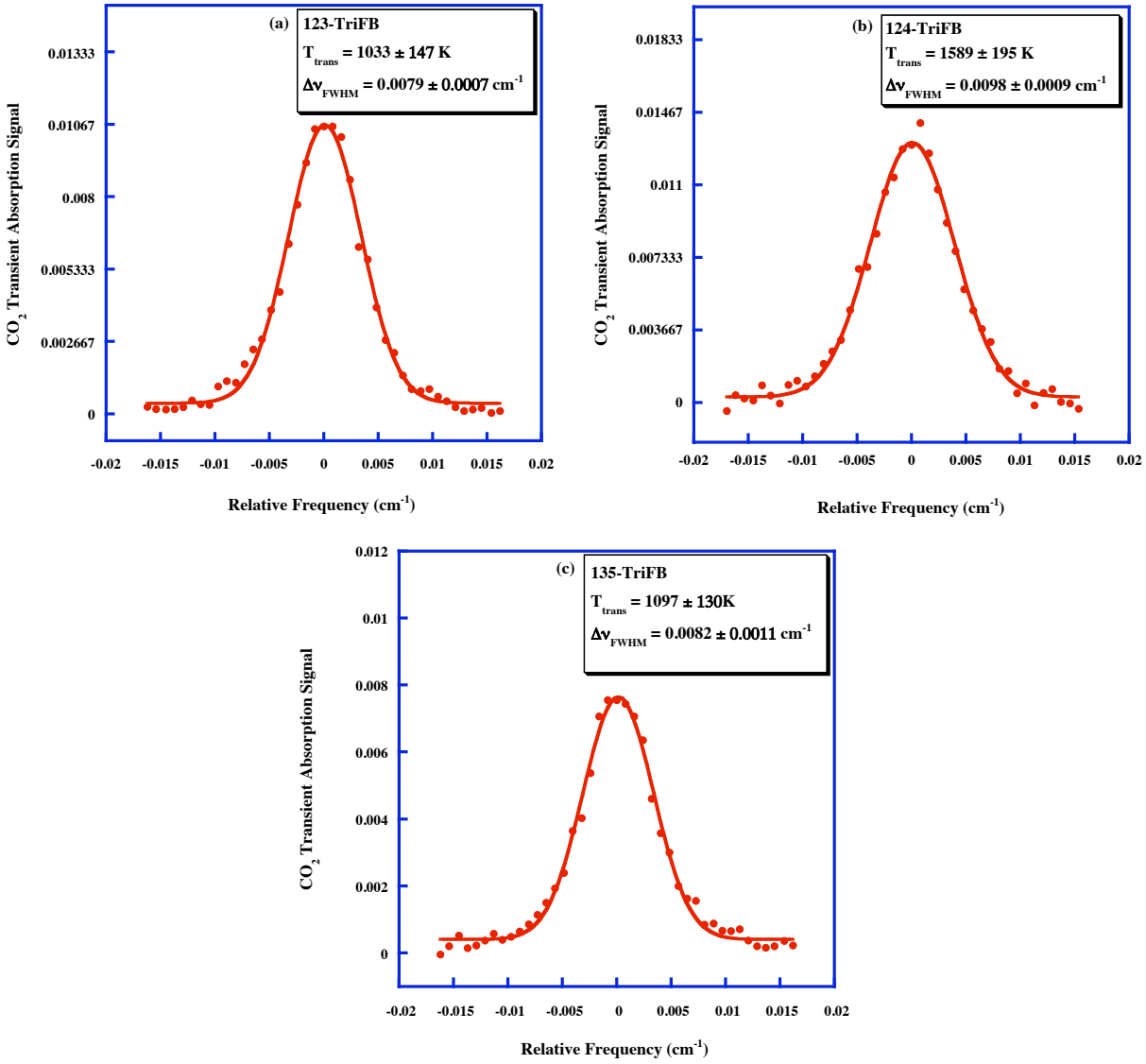
(a)
123-TriFB
T_{trans} = 1033 ± 147 K
$\Delta\nu_{FWHM}$ = 0.0079 ± 0.0007 cm^{-1}
CO_2 Transient Absorption Signal
0.01333
0.01067
0.008
0.005333
0.002667
0
-0.02 -0.015 -0.01 -0.005 0 0.005 0.01 0.015 0.02
Relative Frequency (cm^{-1})
(b)
124-TriFB
T_{trans} = 1589 ± 195 K
$\Delta\nu_{FWHM}$ = 0.0098 ± 0.0009 cm^{-1}
CO_2 Transient Absorption Signal
0.01833
0.01467
0.011
0.007333
0.003667
0
-0.02 -0.015 -0.01 -0.005 0 0.005 0.01 0.015 0.02
Relative Frequency (cm^{-1})
(c)
135-TriFB
T_{trans} = 1097 ± 130K
$\Delta\nu_{FWHM}$ = 0.0082 ± 0.0011 cm^{-1}
CO_2 Transient Absorption Signal
0.012
0.01
0.008
0.006
0.004
0.002
0
-0.02 -0.015 -0.01 -0.005 0 0.005 0.01 0.015 0.02
Relative Frequency (cm^{-1})

and 1097 K, respectively. These linewidths are about two times the value obtained for a room temperature distribution of CO_2 (0.0042 cm^{-1}) signifying that a large amount of vibrational energy is being transferred from the donor and converted to translational energy in CO_2.

Linewidths for CO_2 J=58 to J=80 were measured and are tabulated in Table 3.1 along with lab frame and center of mass frame translational temperatures corresponding to each linewidth. Translational temperatures are given in both lab frame and center of mass frame since the center of mass frame more accurately describes the amount of energy transferred in each collision and are also necessary to calculate *P(E,E')* from the data. Figure 3.4 graphically shows the translational temperatures plotted vs. J state; the right axis gives the center of mass temperatures while the left axis plots FWHM in wavenumbers. An overall direct correlation between J state and translational temperature for scattered CO_2 indicates that higher J states have a larger distribution of velocities or larger temperatures; the linear relationship is the result of a constant impact parameter over these J-states.[29]

3.3.2 State-Resolved Scattering Energy Transfer Rate Constants and Probabilities.

Rate constants for scattering into each state following a collision with 124-TriFB are calculated at 1 μsec, much less than the mean gas kinetic collision time and thus represent the rate and probability of single collision events. The expression

(3.1)

is used to calculate this rate constant where [CO_2 (00^00J,V)] is the concentration of CO_2 molecules excited into a specific state obtained through infrared absorption measurements, $[CO_2]_0$ is the initial number of CO_2 molecules obtained through pressure, and $[TriFB^{E'}]_0$ is the number of TriFB molecules excited to energy E′ found through UV absorption. This

Table 3.1: Full width at half maximum Doppler linewidths,[a] translational temperatures,[b] and center of mass translational temperatures[c] for $CO_2(00^00, J)$ following collisions with highly vibrationally excited 1,2,3-trifluorobenzene[E'], 1,2,4-trifluorobenzene[E'], and 1,3,5-trifluorobenzene[E'].[d]

CO_2	1,2,3-trifluorobenzene			1,2,4-trifluorobenzene			1,3,5-triifluorobenzene		
$(00^00,J)$[e]	$\Delta\nu_{obs}$, (cm^{-1})[a]	T_{trans}, K[b]	T_{trans}^{COM}, K[c]	$\Delta\nu_{obs}$, (cm^{-1})[a]	T_{trans}, K[b]	T_{trans}^{COM}, K[c]	$\Delta\nu_{obs}$, (cm^{-1})[a]	T_{trans}, K[b]	T_{trans}^{COM}, K[c]
58	0.0058±0.0001	560±5	650±5	0.0076±0.0014	930±140	1140±170	0.0056±0.0004	510±20	580±20
62	0.006±0.001	620±60	730±70	0.0089±0.0017	1300±100	1630±130	0.0055±0.0005	500±20	570±20
66	0.0070±0.0003	810±20	980±30	0.0087±0.002	1260±130	1570±160	0.0076±0.003	970±150	1190±180
70	0.0079±0.0005	1030±60	1280±80	0.0098±0.0009	1430±100	1810±120	0.008±0.001	1100±130	1360±160
76	0.009±0.001	1470±80	1860±100	0.0101±0.001	1610±170	2040±230	0.010±0.002	1620±100	2060±130
80	0.010±0.001	1780±190	2280±250	0.0121±0.0007	2430±60	3140±70	0.012±0.002	2420±280	3130±360

Table 3.1 continued

[a] The measured full width at half maximum of the transient Doppler linewidths for the translations $CO_2(00^00,J) \rightarrow CO_2(00^01,J-1)$, determined at 1 μs after trifluorobenzene excitation in a 1:1 sample of trifluorobenzene:CO_2 at a total pressure of 20 mTorr. The thermal Doppler linewidth for CO_2 at T=298 K is $\Delta\nu_0$ =0.0042 cm^{-1}. [b] The final translational temperature, T_{trans}, is obtained from fitting the experimentally determined Doppler lineshapes with a Gaussian function, and it is related to the linewidth, $\Delta\nu_0$ (full width at half maximum) through the expression $T_{trans}(K)=[mc^2(\Delta\nu_{obs})^2]/[8Rln2(\nu_0)^2]$, where m is the mass of CO_2, c is the speed of light, R is the gas constant, and ν_0 is the wavenumber at the center of the absorption line. [c] The final center of mass temperature, T_{trans}^{COM}, is obtained from the expression $T_{trans}^{COM}(K) = T_f^{CO_2} + (T_f^{CO_2} - T)(m_{CO_2}/m_{trifluorobenzene})$, where $T_f^{CO_2}$ is the temperature describing the CO_2 lab frame velocity, T is the ambient cell temperature, and m is the mass of CO_2 and trifluorobenzene, respectively. [d] The internal energy of 1,2,3-trifluorobenzene is E'=41276 cm^{-1}, 1,2,4-trifluorobenzene is E'=41200 cm^{-1}, and 1,3,5-trifluorobenzene is E'=41192 cm^{-1}. [e] The final CO_2 rotational energy state following collision with vibrationally excited donor.

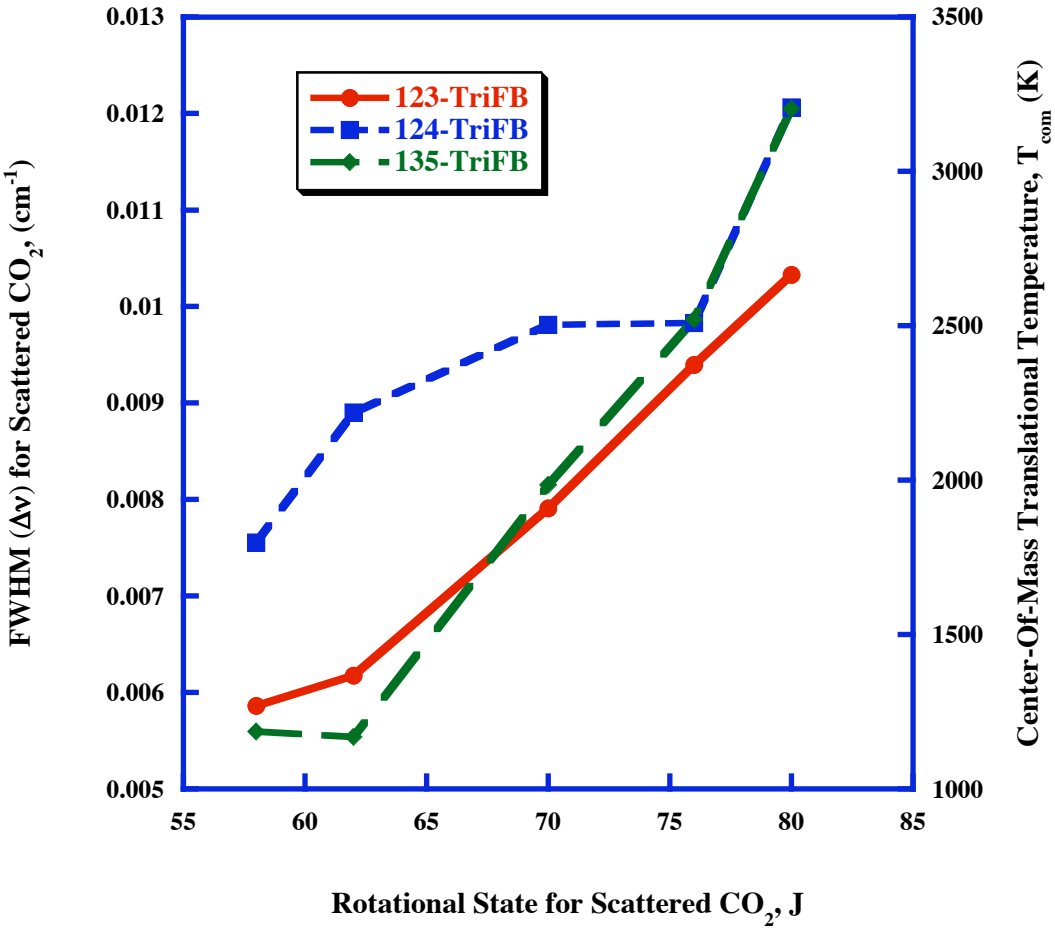

Figure 3.4: The FWHM Doppler linewidth of absorption transitions probing high rotational states (J=58-80) of CO_2 following collisions with vibrationally hot 1,2,3- TriFB (red), 1,2,4-TriFB (blue) and 1,3,5-TriFB (green) is plotted against the final rotational state J. The linewidth in wavenumbers is plotted on the left axis and center of mass translational temperatures determined from the measured linewidths are given on the right y-axis. The linewidths are measured 1 μsec following 248 nm excimer laser excitation of the TriFB, insuring that the measured velocity distributions are the result of single collisions between CO_2 and TriFB ($\tau_{coll} \approx 4$ μsec). The plot shows that T_{com} increases monatonically with final J state.

method can only be used for 124-TriFB because eq 3.1 assumes that infrared absorption is linear with time over the first few microseconds. As seen in Figure 3.1, the linear relationship breaks down with 123 and 135-TriFB. This indicates that other collision events must be taken into account in order to find the rate constant. Mullin et al.[30] faced a similar challenge in the measurement of pyridine relaxation. Following their work, a brief outline will be shown that leads to accurate measurements of the rate of CO_2 scattering into a specific J state. Taking all possible pathways at early times into account gives the following rate equation showing the relationship between excited bath molecules and time

$$\begin{aligned}\frac{d\left[\mathrm{CO}_2^*(J)\right]}{dt} = k_2^J\left[\mathrm{CO}_2\right]\left[\mathrm{TriFB}^*\right] - k_{q4}\left[\mathrm{CO}_2^*(J)\right][M] \\ + k_{q5}\left[\mathrm{CO}_2^*(J'')\right][M] - k_{q6}\left[\mathrm{CO}_2^*(J)\right]\end{aligned} \tag{3.2}$$

where k_2^J is the rate of scattering into a specific J state, k_{q4} is the rate of quenching of CO_2^* through a collision with any other molecule in the cell, k_{q5} is the rate of quenching CO_2^* that has more energy than J state being probed and the resulting CO_2 is in the J state of interest, and k_{q6} represents the loss of CO_2^* due to molecules that have moved out of the beam path. M represents any molecule in the reaction cell. The time dependence of excited TriFB is given by

$$[\mathrm{TriFB}^*](t) = [\mathrm{TriFB}^*]_0 \exp\{-(k_{q1}[\mathrm{CO}_2]_0 + k_{q2}[\mathrm{TriFB}]_0)t\} \tag{3.3}$$

where k_{q1} is quenching of $TriFB^*$ by CO_2 and k_{q2} is quenching of $TriFB^*$ by TriFB.

Integration of eq 3.2 over time and using relationships found in eq 3.3 gives the following equation

$$\frac{\left[CO_2^*(J)\right]}{\left[CO_2\right]_0\left[TriFB^*\right]_0} = \frac{k_2^J}{k_{q1}\left[CO_2\right]_0 + k_{q2}\left[TriFB\right]_0} \times\left(1-\exp\left\{-\left(k_{q1}\left[CO_2\right]_0 + k_{q2}\left[TriFB\right]_0\right)t\right\}\right) \tag{3.4}$$

Equation 3.4 is valid at early times after UV excitation and describes the population of $CO_2^*(J)$ with time. The final step is taking the derivative of eq 3.4 with respect to time to give

$$\frac{d}{dt}\left[\frac{[\mathrm{CO}_2^{*J}]}{[\mathrm{CO}_2]_0[\mathrm{TriFB}^*]_0}\right] = k_2^J \exp\{-(k_{q1}[\mathrm{CO}_2]_0 + k_{q2}[\mathrm{TriFB}]_0)t\}. \tag{3.5}$$

Plotting the natural log of the left hand side of eq 3.5 vs. time yields a straight line with the y-intercept $b = \ln\left(k_2^J\right)$.

Following this method, $[CO_2(00^00,J,V)]/([CO_2]_0[TriFB^{E'}]_0)$ was calculated for all transient data points and fit to a third order polynomial over the first 4 μsec following laser excitation. A third order polynomial is chosen so as not to bias the fit towards the exponential of eq 3.4. An example of this fitting routine is shown in Figure 3.5 where $[CO_2(00^00,J=70,V)]/([CO_2]_0[123\text{-}TriFB^{E'}]_0)$ is plotted vs. time, shown in the solid red line, while the fit to a third order polynomial is shown by the dashed blue line. Taking the natural log of the derivative of this function and finding the intercept of its linear fit produces the rate of scattering into the specified J state through a single collision.

Rate constants from collisions between hot (E´ ≈ 40,000 cm^{-1}) TriFB with CO_2 are given in Table 3.2. These rate constants are scaled using the method described in the experimental section where experiments with pyrazine/CO_2 are scaled to literature values[20] and the same scaling is then applied to these rate constants. Table 3.2 also

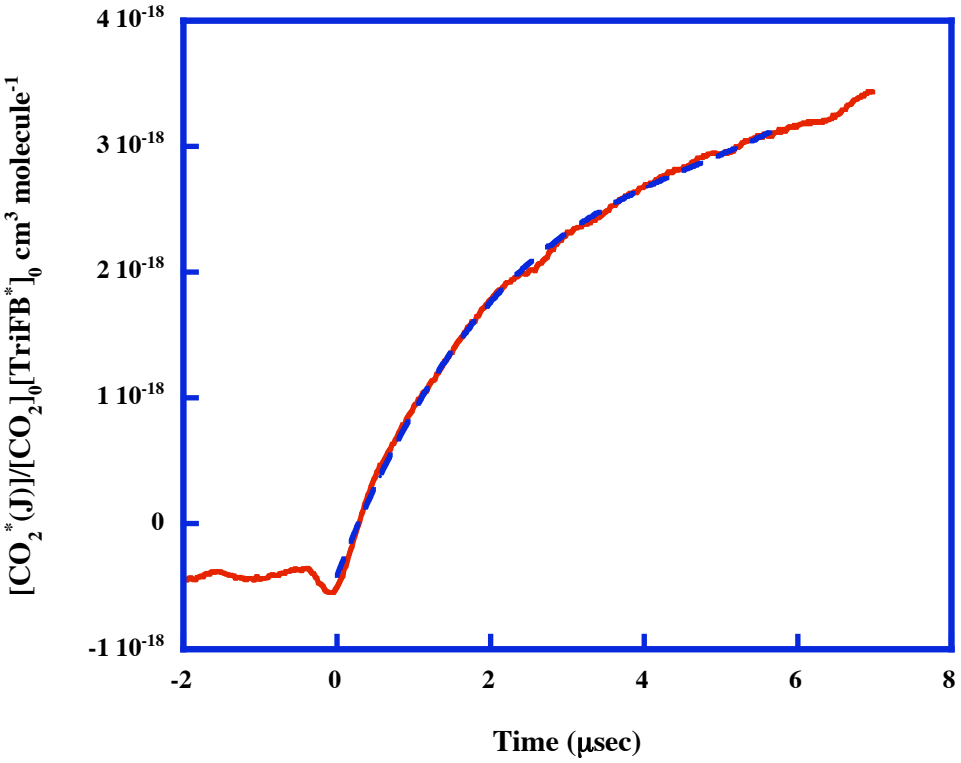

Figure 3.5: $[CO_2(00^00,J=70,V)]/([CO_2]_0[123\text{-}TriFB^{E'}]_0)$ is plotted in red versus time and the best fit third order polynomial over the first 4 μsec following the excitation laser pulse in blue. After 4 μsec, the fit deviates from the data as additional types of reactions that are not accounted for in the fit occur. The fit is used to calculate the rate of scattering CO_2 into a specific J state as described following eq 3.2.

Table 3.2: State-specific energy transfer rate constants $\left(k_2^J\right)$ and probabilities[a] $\left(k_2^J/k_{LJ}\right)$ for the energy transfer process trifluorobenzene$^{E'}$ + $CO_2(00^00)$→trifluorobenzene^{E} + $CO_2(00^00,J,V)$.

CO_2 $(00^00,J)$	k_2^J $(10^{-12}$ cm^3 molecule^{-1}s$^{-1})$		
	1,2,3-triflurobenzene	1,2,4-trifluorobenzene	1,3,5-trifluorobenzene
58	9.5±3.1	5.6±0.4	10.6±8.2
62	7.4±0.8	4.1±0.3	3.8±0.8
66	6.7±2.4	2.3±0.4	
70	4.4±0.6	2.2±0.5	2.2±0.3
76	2.8±0.4	1.3±0.1	1.5±0.9
80	2.6±1.0	1.2±0.1	2.0±1.0
J_{final}	k_2^J/k_{LJ} (10^{-3})		
58	18.3±6	10.7±0.7	20.5±15.8
62	14.2±2	7.9±0.6	7.2±1.7
66	12.9±5	4.3±0.7	
70	8.5±1	4.2±0.7	4.2±0.6
76	4.0±1	2.4±0.1	2.9±1.7
80	3.8±2	2.3±0.3	3.8±1.9

Table 3.2 continued

[a] The probability for energy transfer is given as $Prob_{LJ} = k_2^J / k_{LJ}$, where k_{LJ} is the Lennard-Jones has kinetic collision rate constant. It is defined (see Ref. 31) as $k_{LJ} = \pi\left[\left(d_{CO_2} + d_{trifluorobenzene}\right)/2\right]^2 \sqrt{(8k_BT)/(\pi\mu)}\Omega_{12}$, where d_{CO_2} = 4.5Å, Ref. 32, $d_{trifluorobenzene}$ = 5.4 Å (assumed to be equal to benzene, Ref. 32), k_B is Boltzmann's constant, and μ is the reduced mass. Ω_{12} is the Lennard-Jones collision integral given by the following expression:[2] $\Omega_{12} = \left[0.636 + 0.567\log(kT/\varepsilon_{12})\right]^{-1}$, where ε_{12} is trifluorobenzene-CO_2 well depth with ε_{CO_2}/k =195 K, (Ref. 32), $\varepsilon_{1,2,3TriFB}/k$ =423 K, $\varepsilon_{1,2,4TriFB}/k$ =418 K, and $\varepsilon_{1,3,5TriFB}/k$ =400 K (Ref. 33), and $\varepsilon_{12} = \sqrt{\varepsilon_{CO_2}\varepsilon_{trifluorobenzene}}$. The Lennard-Jones collision rate constants at 298 K for the three isomers of trifluorobenzene are $k_{LJ(1,2,3TriFB)} = 5.22 \times 10^{-10}$, $k_{LJ(1,2,4TriFB)} = 5.24 \times 10^{-10}$, and $k_{LJ(1,3,5TriFB)} = 5.19 \times 10^{-10}$ cm^3 $molecule^{-1}$ s^{-1}.

contains energy transfer probabilities representing the probability of a CO_2 molecule being scattered into a particular J state following a collision with TriFB, obtained using

(3.6)

where the experimental rate constant is divided by the Lennard-Jones rate constant. Although Lennard-Jones almost certainly does not give an accurate description of the intermolecular potential and thus the collision rate constant, using it as a theoretical collision rate constant provides the benefit of allowing these results to be comparable to those of previous studies and also allows energy transfer events between the group of TriFB donors to be compared. A detailed discussion[12] of using the Lennard-Jones rate constant as a scaling factor of energy transfer probability has been given elsewhere.

3.3.3 Energy Transfer Probability Distribution Function.

The rate constants and energy transfer probabilities obtained in this study are indexed according to CO_2 rotational states; energy transfer probability can be resorted as a function of E − E′ to obtain *P(E,E′)*[34] where E′ is the precollision energy of the donor and E is the final energy of the donor following a single collision between donor and bath. Figure 3.6 plots *P(E,E′)* vs. E − E′. Because comparisons of *P(E,E′)* for different donor/bath systems are difficult, a model function has been used in previous studies to simplify this evaluation. Previous work[5,12,13,15,34] has shown that a single exponential function is not sufficient to adequately describe the relationship between probabilities and their corresponding energy transfers given the constraints of normalization and detailed balance; therefore, a normalized double exponential function developed by Troe[19] that fits the data with greater

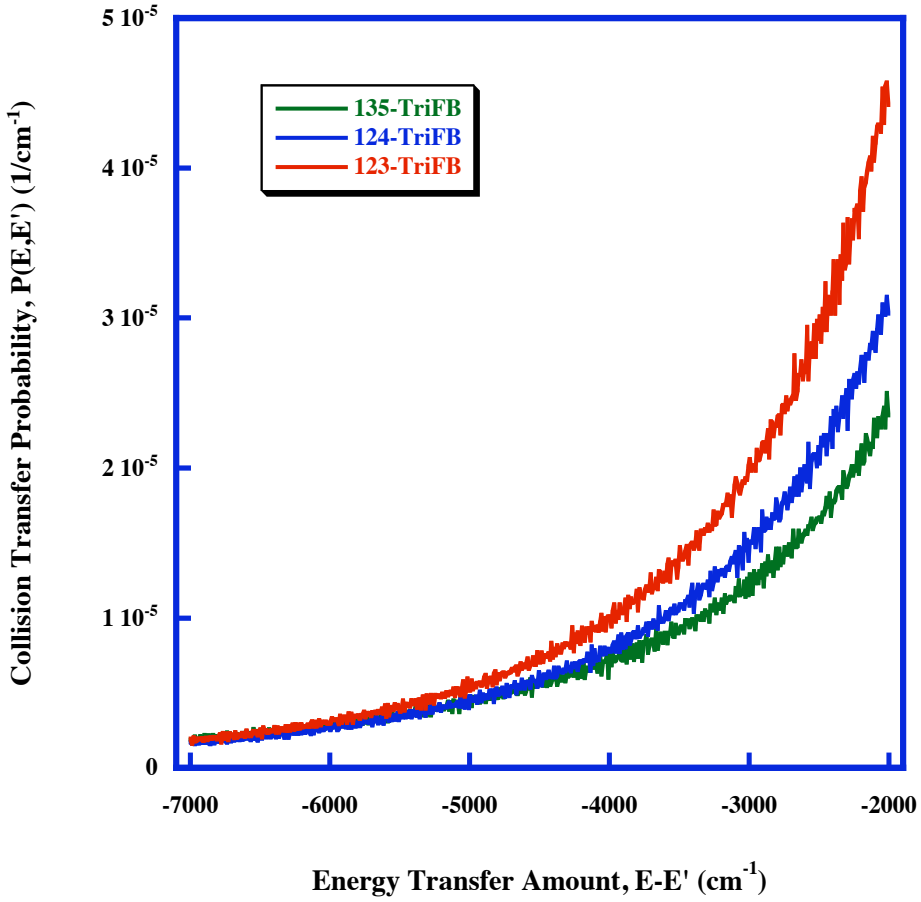

Figure 3.6: Shown are plots of the large ΔE tail of the energy transfer probability distribution function, P(E,E') describing the first Lennard-Jones collision between vibrationally excited 1,2,3,- TriFB (red), 1,2,4,-TriFB (blue) and 1,3,5-TriFB (green) at energy E' ≈ 41,000 cm^{-1} and a CO_2 bath molecule resulting in CO_2 excitation into high rotational angular momentum states (J = 58 - 80) of the ground vibrational level.

accuracy, given the constraints, has been used. Figure 3.7 displays both the experimental *P(E,E')* and the fit of the double exponential function using a logarithmic scaled y-axis.

The downward collision probabilities are described by the bi-exponential function according to

$$P(E,E') = \frac{(1-f)\exp\{-(E'-E)/\alpha\} + f\exp\{-(E'-E)/\gamma\}}{(1-f)(\alpha+\beta)+f(\gamma+\delta)} \qquad E \le E' \tag{3.7}$$

The characteristic energy for downward "weak" collisions is represented by α, while downward "strong" (or super) collisions are given by γ. Upward collision energies are given by the parameters β and δ for the respective weak and strong collisions, where β and δ are related to α and γ by detailed balance.[19] The parameter *f* is related to the number of strong collisions. Although not strictly a "fraction", it does relate the number of strong collisions to the number of weak collisions and increases as the number of supercollisions increase. Another equation relating upward collisions is similar in form to eq 3.7 with the exchange of E for E′, β for α, and δ for γ. Fitting the up collision (small ΔE) region is not required as detailed balance is used to obtain up collision parameters from the fitted down collision parameters.

3.4 Discussion

The study of relaxation of the trifluorobenzene isomers via collisions with CO_2 is a continuation of a comprehensive study of all the fluorinated benzenes to find molecular parameters that influence the shape and magnitude of *P(E,E')* such as density of states, number of low frequency modes, and dipole moments. Considering the group of TriFB isomers, Table 3.2 shows that probability in general increases with dipole moment.

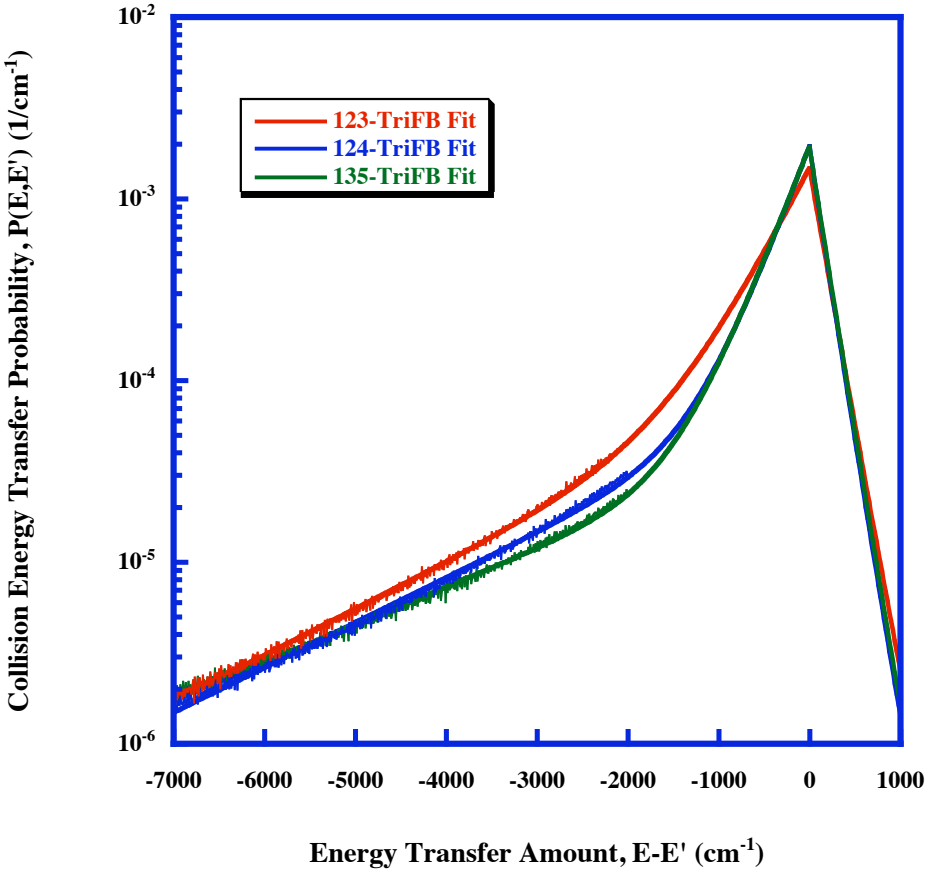

Figure 3.7: Plot (noisy line) of P(E, E') for 1,2,3- TriFB (red), 1,2,4,-TriFB (blue) and 1,3,5-TriFB (green) with CO_2 and E' ≈ 41,000 cm^{-1} along with the best-fit biexponential model functions (Eq 3.7) (solid line). The P(E,E') shown is calculated based on the estimated value of $<J_i>$=28.7 for the mean initial rotational state, J_i, for collisions populating high J_f states (J_f = 58 - 80) of CO_2.

However, for some rotational states, the energy transfer probability is not drastically different; some being the same within the error. Contrast this with the CO_2 transient signal following excitation (see Figure 3.1) of the three TriFB isomers. Initially, it appears that these molecules would have extremely different behaviors, but the transient is only representative of the number of CO_2 molecules excited into a specific rotational state. It does not account for the number of excited donor molecules that were available for collisions. Interestingly, each molecule absorbed 248nm UV light much differently with 135-TriFB hardly absorbing any at all. This lack of absorption by the donor is the underlying reason for such low CO_2 transient signals for this molecule. With all factors accounted for and using the fitting routine discussed earlier, reasonable values emerged that are similar to those of previous studies.[13,25] Large uncertainties for 135-TriFB are a result of low absorption. However, confidence is gained in the results since the TriFB rate constants and probabilities have similar trends as those seen in previous studies[13,25] of other fluorinated benzene molecules. Greater accuracy might be found by using a different excitation wavelength where the donor has a larger absorption coefficiant, but this would change internal energy and other dependent parameters making comparisons more difficult.

An assessment of the TriFB isomers as they compare to similar molecules requires the use of the double exponential function fit to $P(E,E')$ using eq 3.7. Parameters acquired through this fit can be found in Table 3.3 and give insight to strong and weak collisions as well as how they relate to each other. Similar molecules are also included in the table and will be considered in this study are MFB[24], DFB[13], TetraFB[25], and C_6F_6.[5] Other molecular properties that have been shown to influence $P(E,E')$ are included in the table; these

Table 3.3: The downward collision bi-exponential fit parameters (γ^a, α^b, f^c, and $\langle \Delta E \rangle_d^d$) for the experimentally obtained large ΔE tail of *P(E,E′)*, as well as several molecular parameters comprising initial energy E′, molecular dipole moments, the pre-collision state density, and the number of vibrational modes with frequency less than 500 cm^{-1} for various fluorinated benzene donors.

Donor	γ^a (cm^{-1})	α^b (cm^{-1})	f^c	$\langle \Delta E \rangle_d^d$ (cm^{-1})	Initial Energy, E′ (cm^{-1})	Dipole moment[e] (D)	ρ(E′)[f]	s < 500[g] cm^{-1}
C_6H_5F [h]	1924	298	0.03	574	40,843	1.66	2.9×10^{16}	4
12-DFB [h]	1850	343	0.06	739	41,025	2.59	5.7×10^{17}	5
13-DFB [h]	2061	295	0.03	638	41,011	1.51	5.2×10^{17}	5
14-DFB [h]	2408	294	0.03	713	41,019	0	5.5×10^{17}	6
123-TFB	1705	434	0.070	724	41,276	~3.70	2.7×10^{19}	7
124-TFB	1757	321	0.041	593	41,200	1.39	1.0×10^{19}	7
135-TFB	2106	334	0.025	581	41,192	0	9.4×10^{18}	7
1234-TFB [h]	1796	391	0.06	688	41,274	2.42	4.7×10^{19}	8
1235-TFB [h]	1886	376	0.05	672	41,403	1.46	2.7×10^{20}	8
1245-TFB [h]	1617	380	0.05	594	41,395	0	2.3×10^{20}	10
C_6F_6 [h]	1411	620	0.15	847	41,822	0	2.1×10^{23}	13

Table 3.3 continued

[a] The characteristic strong energy transfer magnitude as determined from the biexponential fit of the *P(E,E')* data. [b] The characteristic weak energy transfer magnitude as determined from the biexponential fit of the *P(E,E')* data. [c] The "fraction" of strong collisions as determined from the biexponential fit of the *P(E,E')* data. [d] The average energy transferred in a single downward collision involving a vibrationally excited donor and CO_2. determined using the biexponential fit paramters according to $\langle \Delta E \rangle_d = (\alpha^2(1-x) + \gamma^2 x)/(\alpha(1-x) + \gamma x)$. [e] Molecular dipole moments obtained from Ref 35. [f] The vibrational density of states for the donor molecule at the energy following the absorption of a 248 nm photon calculated using the Whitten—Rabinovitch algorithm (Ref 36). [g] The number of vibrational normal modes with frequencies less than 500 cm^{-1}. Normal-mode frequencies for C_6F_6 are from Refs 37 and 38, TetraFB isomers are obtained from Refs 37 and 39, and TriFB isomers from Refs 37 and 40. [h] *P(E,E')* parameters for MFB, DFB, TetraFB, and C_6F_6 obtained from Refs 24, 13, 25, and 5, respectively.

properties include dipole moment, initial energy, density of states, and number of low frequency modes(<500 cm^{-1}).

Our lab presented research[12] that linked the number of low frequency modes to the "fraction" (*f*) of strong equations from eq 3.7. Based on those results, similar fractions would be predicted for all TriFB isomers as each have the same number of modes below 500 cm^{-1}. Table 3.3 shows that the three TriFB isomers have three different strong collision "fractions" even though the number of low frequency modes has not changed. This would suggest that either the number of low frequency modes is not the only parameter to effect a change on the "fraction" of strong collisions or the two have been coincidently linked by previous studies.

Previous studies[15] have shown that *P(E,E')* is related to the donor molecule state density; in particular the way in which the donor state density changes with internal energy. This can be done by evaluating the slope of the natural log of a molecule's density of states as function of internal energy and comparing this to the shape of *P(E,E')* represented by its biexponential fit parameters. By using an application of Fermi's Golden rule, the equation

$$P(E,E') \propto \left|V_{if}\right|^2 \rho(E)\rho(E') \qquad (3.8)$$

connects *P(E,E')* with density of states. In the equation, V_{if} is the matrix element $\langle i \left| H \right| f \rangle$ which links the initial and final states, and *ρ(E)* and *ρ(E')* is the density of states at *E* and *E'*, respectively, the donor energy before and after collisions. Equation 3.8 indicates that *P(E,E')* is directly proportional to the donor's final density of states(it is also directly proportional to the initial donor state density but another study found this to be constant); thus the shape of *P(E,E')* how it changes with E, should mirror the shape of ρ(E). Figure 3.8

plots the shape of *P(E,E′)*, given according to the inverse fitting parameters for strong and weak collisions obtained from the fit of the experimentally determined *P(E,E′)* to eq 3.7 which is the slope of the natural log of *P(E,E′)*, vs. the slope obtained by plotting the natural log of the density of states versus final donor energy, E. From left to right, the data points are MFB, three DFB isomers, three TriFB isomers, three TetraFB isomers, and C_6F_6. A strong linear fit is observed for the gamma parameters as is expected considering the experiment measures the strong collision energy transfer events directly; alpha, weak energy transfer parameter, also shows a good fit, especially when considering that this portion of *P(E,E′)*, the small ΔE tail, is extrapolated based on experimental results. 135-TriFB has a value for α that is well below the line; in this case, large uncertainties in the experimental data compounded uncertainties in extrapolation, causing a value much lower than would be predicted. As discussed elsewhere,[13] because low frequency modes effect the state density most, the results of Figure 3.8 support the notion that low-frequency motion is most responsible for the shape of *P(E,E′)*.

Quantum scattering and classical trajectory studies has further shown that low frequency modes had the largest energy transfer cross sections, indicating more energy is transferred in a single collision. Clary *et al.*[22] used quantum scattering calculations to study the relaxation of benzene via collisions with He; the study not only showed that low frequency modes were important, but also showed the motion of the molecule to be an important aspect. The frequency of ν_6, a stretching mode with higher frequency than ν_{16}, was altered such that its frequency was the same as ν_{16}, a lower frequency bending mode. The study found that ν_{16} still had a larger energy transfer cross section, indicating that bending motions are more efficient at transferring energy, even when the frequency of is

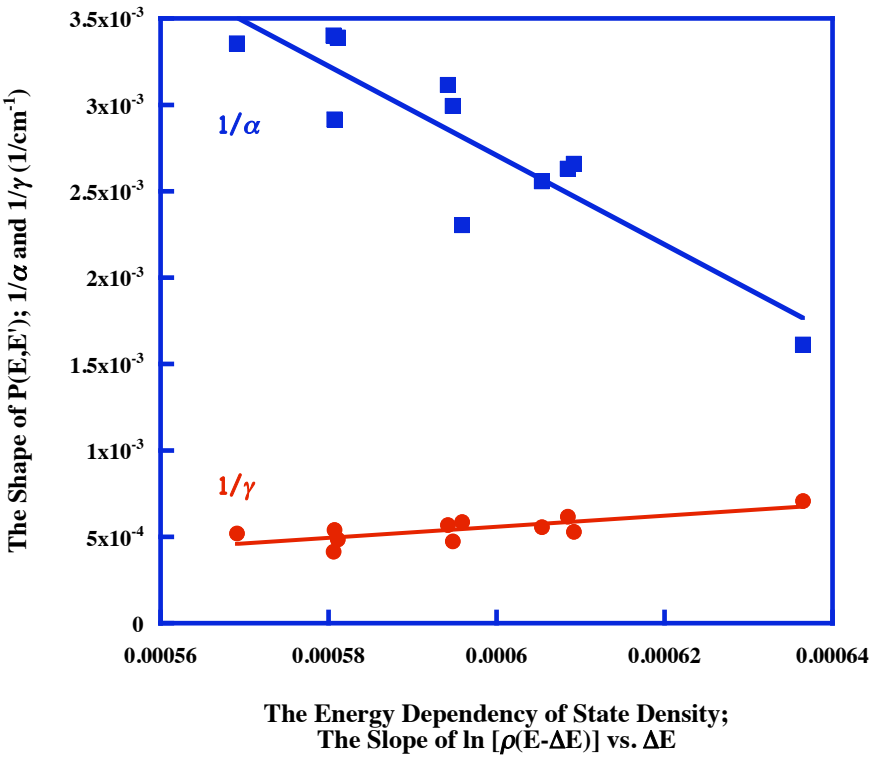

Figure 3.8: The correlation between the shape of P(E,E') as determined by the biexponential fit parameters ($1/\alpha$ and $1/\gamma$) and the energy dependent state density of the donor molecules. Circles represent the characteristic energy transfer magnitude for "strong" collisions (γ) while the squares are the characteristic energy transfer magnitude for "weak" collisions (α). Based on the application of Fermi's Golden Rule to collisional deactivation of vibrationally excited donor molecules in collisions with CO_2. From left to right in the figure data points are for monofluorobenzene, the three difluorobenzenes, the three tetrafluorobenzenes, and C_6F_6. Monofluorobenzene, difluorobenzenes, and C_6F_6 data are from Refs (5, 15, 34). The shape of the energy transfer distribution function as a function of ΔE mirrors the shape of the final donor density of states as a function of energy transferred (ΔE). The shape of both the strong and weak collision region of P(E,E') is correlated with the donor molecule's final density of states.

modes identical. In addition to identifying what motion ultimately effects *P(E,E′)*, Clary's study also indicated that only 3 modes ν_6, ν_{11}, and ν_{16} had significant energy transfer cross sections and are most responsible for energy transfer in a collision. These modes have been described as "gateway modes" by Lendvay[23] and are where a majority of the energy is leaked to the bath. Gateway modes can be identified experimentally. This requires the use of a model developed by Sevy *et al.*[15] and is referred to as the "fractional energy transfer distribution model". This model relates *P(E,E′)* to an efficiency factor, related to the frequency of the mode, and the fraction of molecules in the mode that have sufficient energy to transfer. Fractional mode analysis has been performed in several previous studies[12,13,15] where its methods are detailed. By analyzing the modes, agreement with these previous studies can be identified leading to an improved understanding of how the frequency of certain modes affect *P(E,E′)*. Figure 3.9 graphically shows the fraction of molecules for modes that are either low frequency (<500 cm^{-1}) or have out-of-plane motion with at least 2000 cm^{-1} (3.9a), 5000 cm^{-1} (3.9b), and 8000 cm^{-1} (3.9c) in energy. Table 3.4 presents the frequency of the modes listed on the plot. The mode assignments in both the figure and table are given using Wilson notation,[41] which is used for benzene-like molecules and assigns modes based on motion; these mode assignments do not change with point group making these assignments ideally suited for this study where 123-TriFB is C_{2v}, 124-TriFB is C_{1h}, and 135-TriFB is D_{3h}.

The analysis points to ν_{11} and ν_{16} as the most likely modes to be classified as energy transfer gateways. Comparing 123-TriFB to 124-TriFB reveals 124-TriFB as having a larger frequency for ν_{11}; based on what has been discussed, this should equate into a lower efficiency for that mode in 124-TriFB. Even though the fraction is higher at 8000 cm^{-1}, a

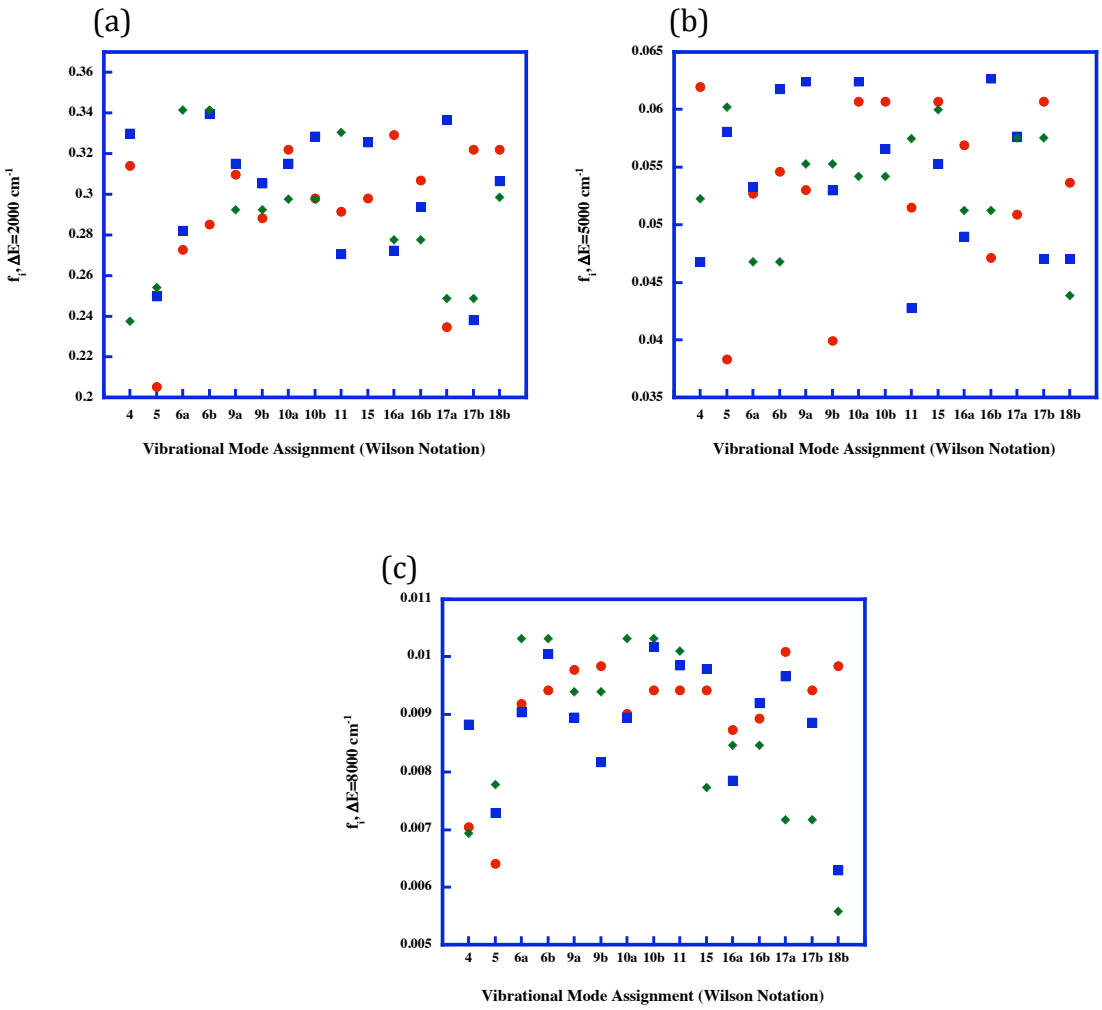

Figure 3.9: Fractional mode populations for highly vibrationally excited (E'~41,000 cm^{-1}) for 1,2,3-TriFB (red), 1,2,4-TriFB (blue), and 1,3,5-TriFB (green) with at least (a) 2000 cm^{-1}, (b) 5000 cm^{-1}, and (c) 8000 cm^{-1}. The x-axis is the vibrational mode assignment according to Wilson notation, which has been used so that mode assignments represent the same vibrational motion in each molecule. Only the vibrational modes that were determined to be "gateway" energy transfer modes in quantum scattering calculation of the relaxation of benzene by He (ν_{6a}, ν_{6b}, ν_{11}, ν_{16a}, and ν_{16b}) and the remaining out-of-plane or low frequency (<500 cm^{-1}) vibrationalmodes (ν_4, ν_5, ν_{10a}, ν_{10b}, ν_{17a}, ν_{17b}, and ν_{18b}) are included in the figure.

Table 3.4: Fundamental vibrational modes with frequency < 500 cm^{-1} for trifluorobenzene, along with an assignment of the mode motion.

Mode[a]	1,2,3-TriFB[b]	1,2,4-TriFB	1,3,5-TriFB	motion
4	715	688	664	o, ring deform
5	970	856	845	o, C-F bending
6a	480	587	500	ring stretching
6b	580	503	500	ring deform
9a	310	358	326	C-F bending
9b	1150	441	326	C-F bending
10a	210	358	250	o, C-F bending
10b	280	259	250	o, C-F bending
11	760	808	206	o, C-F bending
12	800	781	1010	ring deform
15	280	261	564	C-F bending
16a	515	603	594	o, ring wagging
16b	547	455	594	o, ring wagging
17a	890	156	858	o, C-F bending
17b	140	930	858	o, C-F bending
18b	350	1099	1122	C-F bending
Tot. #	7	7	7	

Table 3.4 Continued

o : out-of-plane motion

a : Wilson notation expression for fundamental vibrational mode[41]

[b] : Motion assignment trifluorobenzene is obtained from Refs. 37 and 40

lower efficiency would cause these two to have similar probabilities as observed in Figure 3.6 in the high ΔE portion of *P(E,E′)*. In Figure 3.9a, the ordering between the two is correct, but the spacing is much larger. With the more efficient and lower frequency mode found in ν_{11} of 123-TriFB, this could easily account for the spacing difference. The 5000 cm^{-1} plot show fractions that do not correspond well at all illustrating the limitation of using what is basically a step function for fractional mode analysis. 135-TriFB has a consistently higher fraction relative to the other TriFB isomers in ν_{11} and ν_{16} which should be efficient low frequency modes; the molecule most likely is simply much weaker at transferring energy over the majority of *P(E,E′)*. This is similar to the result obtained for the 1,4 –DFB in the DFB study and 1,2,4,5-TetraFB in the TetraFB study, all of which are the nonpolar molecule within their respective groups.

Dipole moment has been discussed as having an effect on *P(E,E′)*. Mullin *et al.*[30] investigated the effect of dipole moment on energy transfer by comparing studies of pyrizine, with no dipole moment, to pyridine having a dipole moment of 2.2 D. They found that pyridine had enhanced V→V energy transfer pathways and a slightly diminished V→RT energy transfer pathway that they attributed to pyridine's dipole moment. Later, work by our lab[12] to calculate the *P(E,E′)* for pyridine and compare it to *P(E,E′)* of pyrazine found that the fraction of strong collisions to be much smaller for pyridine, f=0.008. We attributed this diminished number of strong collisions to the enhanced V→V energy transfer pathway described by Mullin, resulting from a large dipole moment. These studies were limited in scope as they only made a single comparison between a molecule with no dipole moment and another molecule with a large dipole moment; the molecules were

similar in form but differed in chemical make-up and mass. Our lab has calculated *P(E,E')* for several groups of fluorinated benzene isomers(DFB, TriFB, and TetraFB) where each group has a different number of fluorine atoms. Within each group, each isomer has a different dipole moments. A link between fraction of strong collisions and dipole moment was not notice for the DFB and TetraFB studies, but these studies along with this study gives 9 molecules in three groups that represent a broad range of dipole moments.

Figure 3.10 plots the fraction of strong collisions found as a fitting parameter obtained through the double exponential for the isomers of DFB, TriFB, and TetraFB against the dipole moment of each of these molecules. The trend indicates that higher dipole moments result in a larger fraction of strong or super collisions. This study showed the strongest correlation between the two parameters and is well suited to make this type of analysis due to similar initial energy, similar motion in the molecules, the same chemical make-up, and large differences in dipole moments between isomers. When DFB and TetraFB isomers are also taken into account, the correlation continues as these molecules show support for an apparent correlation between the fraction of strong collisions and dipole moment. An analysis of the V–V energy transfer pathways in addition to the V–RT pathways for all of these molecules may prove insightful in light of these new findings.

Although the correlation between the dipole moment and *f* looks good for the set of isomers shown in Figure 3.10, C_6F_6 and PFB do not follow this trend; however, they have no other isomers to make comparisons to. The previously discussed link between the "fraction" of strong collisions and number of low frequency modes may still be part of the equation for determining *f*. In the case of DFB, TriFB, and TetraFB, the subtle changes between each group of isomers allows the observation of the finer relationship between

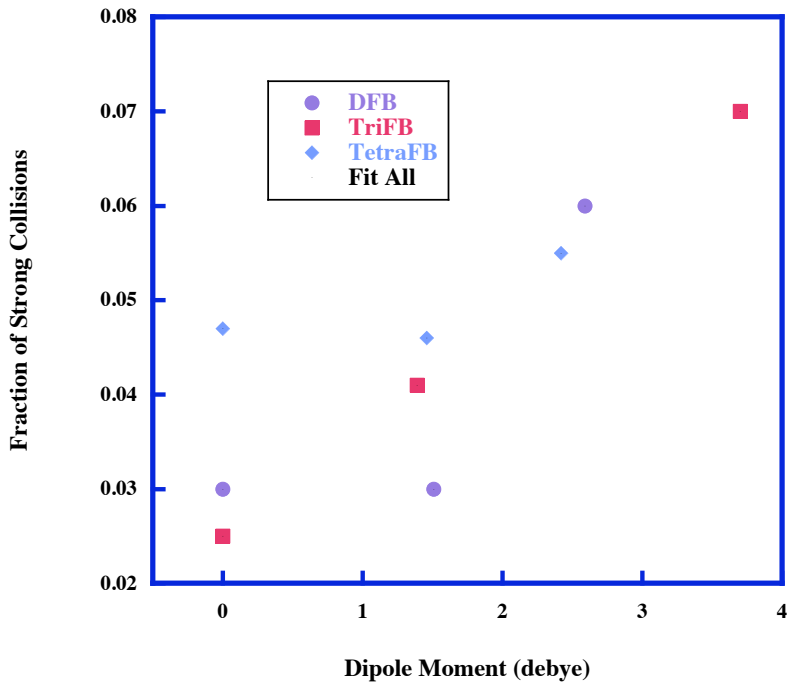

Figure 3.10: Fraction of strong collision parameter as obtained from fitting the double exponential shown in eq 3.7 to *P(E,E')* plotted against dipole moment for DFB, TriFB, and TetraFB. The "fraction" of strong collisions increases with increasing dipole moment. By increasing the fraction of strong collisions, the number of strong or super collision events also increase thus showing the more polar molecules to have greater energy transfer efficiency. DFB and TetraFB data obtained from ref [13] and [25] respectively.

dipole moment and fraction of strong collisions to be observed. Grouping this study with the DFB and TetraFB studies leads to the conclusion that as the dipole increases, relative to other isomers, the fraction of strong or super collisions also increases.

3.5 Conclusion

Collisional relaxation of 123-TriFB, 124-TriFB, and 135-TriFB following collisions with CO_2 was studied using IR diode laser spectroscopy. Bath molecules were probed to determine the amount of energy transferred through a single collision through rotational populations and velocity distributions of the J=58-80 ro-vibrational states of CO_2 of the (00^00) level. Probabilities were sorted according to ΔE to give the energy transfer probability distribution or *P(E,E')* which is then fit to a biexponential function whose shape relates strong and weak collisions. An application of Fermi's Golden rule has shown the shape of *P(E,E')* to correlate with the shape of the donor's state density as a function of energy. Gateway mode analysis identified ν_{11} and ν_{16} as gateqay modes that largely gonvern the shape and magnitude of *P(E,E')*. Dipole moments have also been shown to correlate with the fraction of strong collisions among isomers of similar molecules.

3.6 References

1. Lindemann, F. A., *Transactions of the Faraday Society* **1922,** *17*, 598-606.
2. Troe, J., *J. Chem. Phys.* **1977,** *66*, 4758-4775.
3. Troe, J., *J. Chem. Phys.* **1977,** *66*, 4745-4757.
4. Flynn, G. W.; Weston, R. E., Jr., Glimpses of a Mechanism for Quenching Unimolecular Reactions: A Quantum State Resolved Picture. In *Advances in Chemical Kinetics and*

Dynamics: Vibrational Energy Transfer Involving Large and Small Molecules, Barker, J. R., Ed. JAI Press, Inc.: Greenwich, CT, 1995; Vol. 2B, pp 359-391.

5. Michaels, C. A.; Lin, Z.; Mullin, A. S.; Tapalian, H. C.; Flynn, G. W., *Journal of Chemical Physics* **1996,** *106* (17), 7055-7071.
6. Hold, U.; Lenzer, T.; Luther, K.; Symonds, A. C., *J. Chem. Phys* **2003,** *119*, 11192-11211.
7. Lenzer, T.; Luther, K.; Reihs, K.; Symonds, A. C., *J. Chem. Phys.* **2000,** *112* (9), 4090-4110.
8. Hold, U.; Lenzer, T.; Luther, K.; Reihs, K.; Symonds, A. C., *J. Chem. Phys.* **2000,** *112* (9), 4076-4089.
9. Hippler, H.; Troe, J.; Wendelken, H. J., *J. Chem. Phys.* **1983,** *78* (11), 6709-6717.
10. Toselli, B. M.; Brenner, J. D.; Yerram, M. L.; Chin, W. E.; King, K. D.; Barker, J. R., *J. Chem. Phys.* **1991,** *95* (1), 176-188.
11. Toselli, B. M.; Barker, J. R., *J. Chem. Phys.* **1991,** *95*, 8108-8119.
12. Johnson, J. A.; Kim, K.; Mayhew, M.; Mitchell, D. G.; Sevy, E. T., *Journal of Physical Chemistry A* **2008,** *112* (12), 2543-2552.
13. Mitchell, D. G.; Johnson, A. M.; Johnson, J. A.; Judd, K. A.; Kim, K.; Mayhew, M.; Powell, A. J.; Sevy, E. T., *Journal of Physical Chemistry A* **2008,** *112* (6), 1157-1167.
14. Flynn, G. W.; Weston, R. E., Jr., *Journal of Physical Chemistry* **1993,** *97* (31), 8116-8127.
15. Sevy, E. T.; Rubin, S. M.; Lin, Z.; Flynn, G. W., *Journal of Chemical Physics* **2000,** *113*, 4912-4932.
16. Li, Z.; Korobkova, E.; Werner, K.; Shum, L.; Mullin, A. S., *Journal of Chemical Physics* **2005,** *123* (17), 174306.
17. Havey, D. K.; Liu, Q.; Li, Z.; Elioff, M.; Fang, M.; Neudel, J.; Mullin, A. S., *Journal of Physical Chemistry A* **2007,** *111* (13), 2458-2460.

18. Sevy, E. T. Ph.D. Dissertation. Columbia University, 1999.

19. Troe, J., *J. Chem. Phys.* **1992,** *97*, 288-292.

20. Mullin, A. S.; Michaels, C. A.; Flynn, G. W., *Journal of Chemical Physics* **1995,** *102* (15), 6032-6045.

21. Johnson, J. A.; Duffin, A. M.; Hom, B. J.; Jackson, K. E.; Sevy, E. T., *Journal of Chemical Physics* **2008,** *128*, 054304.

22. Clary, D. C.; Gilbert, R. G.; Bernshtein, V.; Oref, I., *Faraday Discuss.* **1995,** *102*, 423-433.

23. Lendvay, G., *J. Phys. Chem. A* **1997,** *101* (49), 9217-9223.

24. Kim, K.; Johnson, A. M.; Powell, A. L.; Mitchell, D. G.; Sevy, E. T., *Journal of Physical Chemistry A* **In Preparation**.

25. Johnson, A. M.; Mayhew, M.; Kim, K.; Mitchell, D. G.; Powell, A. L.; Hall, L.; Sevy, E. T., *Journal of Physical Chemistry A* **In Preparation**.

26. Sevy, E. T. The Competition Between Photochemistry and Energy Transfer: High Resolution Laser Probes of CO_2 Collision Products and HCN Photoproducts Produced by Highly Vibrationally Excited Azabenzenes. Ph.D. Dissertation, Columbia University, New York, 1999.

27. Pugh, L. A.; Rao, K. N., Intensities from infrared spectra. In *Molecular Spectroscopy: Modern Research Volume II*, Rao, K. N., Ed. Academic Press: New York, 1976; pp 165-227.

28. Rothman, L. S.; Gamache, R. R.; Barbe, A.; Goldman, A.; Gillis, J. R.; Brown, L. R.; Toth, R. A.; Flaud, J. M.; Camy-Peyret, C., *App. Opt.* **1983,** *22*, 2247.

29. Mullin, A. S.; Park, J.; Chou, J. Z.; Flynn, G. W.; Weston, R. E., Jr., *Chemical Physics* **1993,** *175*, 53-70.

30. Wall, M. C.; Stewart, B. A.; Mullin, A. S., *Journal of Chemical Physics* **1998,** *108* (15), 6185-6196.

31. Smith, I. W. M., *Kinetics and Dynamics of Elementary Gas Reactions*. Butterworths: London, 1980.

32. Hirschfelder, J. O.; Curtiss, C. F.; Bird, R. B., *Molecular Theory of Gases and Liquids*. John Wiley & Sons, Inc.: New York, 1954.

33. Lin, H. M.; Seaver, M.; Tang, K. Y.; Knight, A. E. W.; Parmenter, C. S., *Journal of Chemical Physics* **1979,** *70* (12), 5442-57.

34. Michaels, C. A.; Flynn, G. W., *Journal of Chemical Physics* **1997,** *106* (9), 3558-3566.

35. Doraiswamy, S.; Sharma, S. D., *Theochem* **1983,** *94* (1-2), 63-71.

36. Whitten, G. Z.; Rabinovitch, B. S., *J. Chem. Phys.* **1963,** *38* (10), 2466-2473.

37. Eaton, V. J.; Steele, D., *J. Mol. Spec.* **1973,** *48*, 446-458.

38. Pearce, R. A. R.; Steele, D.; Radcliffe, K., *Journal of Molecular Structure* **1973,** *15*, 409-420.

39. Valerie J. Eaton, R. A. R. P., D Steele, and J W Tindle, *Spectrochimica Acta* **1976,** *32A*, 9.

40. Varsanyi, *Assignmens for Vibrational Spectra of Seven Hundred Benzene Derivatives*. John Wiley & Sons: New York, 1974.

41. Wilson, E. B., Jr., *Physical Review* **1934,** *45*, 706-14.